BIOCHEMISTRY
including biophysical chemistry & molecular biology

Article

pubs.acs.org/biochemistry

Ligation of D1-His332 and D1-Asp170 to the Manganese Cluster of Photosystem II from *Synechocystis* Assessed by Multifrequency Pulse EPR Spectroscopy†

Troy A. Stich,[‡,⊥] Gregory J. Yeagle,[‡,⊥] Rachel J. Service,[§] Richard J. Debus,[§] and R. David Britt*[,‡]

[‡]Department of Chemistry, University of California at Davis, One Shields Avenue, Davis, California 95616, United States

[§]Department of Biochemistry, University of California at Riverside, Riverside, California 92521, United States

Supporting Information

ABSTRACT: Multifrequency electron spin-echo envelope modulation (ESEEM) spectroscopy is used to ascertain the nature of the bonding interactions of various active site amino acids with the Mn ions that compose the oxygen-evolving cluster (OEC) in photosystem II (PSII) from the cyanobacterium *Synechocystis* sp. PCC 6803 poised in the S_2 state. Spectra of natural isotopic abundance PSII (^{14}N-PSII), uniformly ^{15}N-labeled PSII (^{15}N-PSII), and ^{15}N-PSII containing ^{14}N-histidine (^{14}N-His/^{15}N-PSII) are compared. These complementary data sets allow for a precise determination of the spin Hamiltonian parameters of the postulated histidine nitrogen interaction with the Mn ions of the OEC. These results are compared to those from a similar study on PSII isolated from spinach. Upon mutation of His332 of the D1 polypeptide to a glutamate residue, all isotopically sensitive spectral features vanish. Additional K_a- and Q-band ESEEM experiments on the D1-D170H site-directed mutant give no indication of new ^{14}N-based interactions.

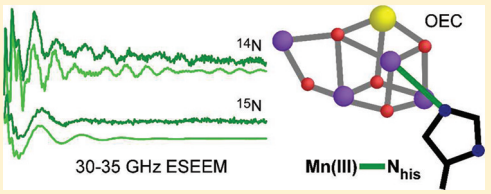

A pentanuclear metal cluster serves at the catalytic site for water oxidation in photosystem II (PSII). This oxygen-evolving complex (OEC) is composed of four Mn ions and one Ca ion bridged to one another via solvent-derived oxo (or hydroxo) bridges. This cluster is presumably bound to the PSII protein by several active-site amino acid residues. Spectroscopic and kinetic studies of PSII prepared with site-specific isotopically labeled amino acids and site-directed mutations have suggested a number of possible candidates for such protein-derived ligands.[2−4] These include D1-Asp170, D1-Glu189, D1-His332, D1-Glu333, D1-His337, D1-Asp342, CP43-Glu354, and the carboxy terminus of the D1 polypeptide at D1-Ala344. The recent spate of X-ray crystal structures of PSII from the thermophilic cyanobacteria *Thermosynechococcus elongatus* and *Thermosynechococcus vulcanus* indicate that all the above residues are indeed near enough to the OEC to be considered within the first coordination sphere.[5−13] However, each of these structures also shows subtle and in some cases significant differences in relative positions of these residues to the Mn cluster. No doubt, these discrepancies are due in large part to the photoreduction of the Mn ions that is known to occur during acquisition of the diffraction data.[14,15] A much higher resolution (1.9 Å) crystal structure was recently reported[a] and was obtained with a lower flux of X-rays combined with crystal slide-oscillation to minimize radiation-induced damage. (The structure has since been deposited in the Protein Data Bank (accession code 3ARC) and discussed in a corresponding paper.[16]) Their model of the OEC and its ligands is consistent with much of the previous crystallographic results. At the time of this writing, however, it is unknown if sufficient resolution exists to make Mn oxidation state assignments. Furthermore, the evolution of this geometry as a function of S state is currently not available from the diffraction data. Thus, there remains a strong need for quantitative characterization of the native protein−OEC bonding interactions.

Electron paramagnetic resonance (EPR) spectroscopy has been a particularly useful tool for characterizing the electronic and geometric structure features of the OEC and does so without deleteriously affecting the protein.[17−26] Of the five S-states of the Kok cycle ($S_0 \cdots S_4$), the best characterized by EPR spectroscopy is the S_2 state. Two distinct EPR signals, both attributed to the OEC in the S_2 state, are detected at X-band (≈9 GHz) excitation frequencies. The first signal consists of 18−22 ^{55}Mn (I = 5/2) hyperfine-induced features and is centered at g = 1.98. This so-called multiline signal (MLS) arises from an S = 1/2 ground spin state of the OEC achieved by a combination of ferromagnetic and antiferromagnetic exchange interactions between the three Mn(IV) ions and one Mn(III) ion.[27−30] The second signal, a derivative-shaped feature centered at g = 4.1, has been assigned to an S = 5/2 ground spin state that arises from an alternative exchange coupling scheme between the four Mn ions.[26,31] Researchers have studied how chemical treatment of PSII-containing preparations (e.g., with small alcohols, fluoride, or ammonia) affects the equilibrium between these two S_2 forms.[32,33] Additional studies have focused on the effect of site-directed mutations on the generation and appearance of the MLS.[34−37]

Received: July 11, 2011
Revised: July 21, 2011
Published: July 26, 2011

These results are crucial to determining the involvement of certain amino acids in securing the OEC to the peptide and tuning its redox properties for proper S-state advancement.

In particular, mutation of D1-His332 to glutamate (D1-H332E) in PSII from *Synechocystis* sp. PCC 6803 abolishes O_2 evolving activity, but short (30 s) illumination at 273 K of dark-adapted (S_1 state) particles leads to formation of a MLS with 24 narrowly spaced peaks (the usual, 8−10 min 195 K illumination procedure surprisingly yields no MLS).[34] These results indicate that the Mn cluster is assembled in these mutants but that the magnetic properties of the OEC are altered. A more detailed insight into the nature of protein−OEC interactions is gained from the application of advanced EPR methods such as electron spin-echo envelope modulation (ESEEM) spectroscopy. ESEEM spectroscopy detects transition frequencies between nuclear spin levels that are hyperfine-coupled to the unpaired electron spin, which, in this case, is localized on the OEC. Early X-band ESEEM studies established that a feature appearing at 4.8 MHz was due to magnetic coupling of a ^{14}N nucleus to the OEC of PSII from *Synechococcus* sp. in its S_2 state.[38] Later studies on *Synechocystis* sp. PCC 6803 that contained histidine residues labeled with ^{15}N at both imidazole nitrogen positions showed a dramatically changed ESEEM spectrum.[39] This nitrogen isotope sensitivity confirms that features observed using X-band ESEEM arise from histidine (though, no new features assigned to coupling from a ^{15}N nucleus were identified). Then an ESEEM study comparing wild-type* and D1-H332E PSII from *Synechocystis* sp. PCC 6803 found that the 4.8 MHz peak decreased or disappeared upon this mutation (see Figure S1).[40,c] A similar feature has now been observed in X-band ESEEM spectra of PSII isolated from higher plants (spinach[40−42] and pea seedlings[43]) as well as mesophilic[38,40] and thermophilic cyanobacteria.[36] Unfortunately, rather little information as to the strength of the magnetic interaction between this histidine nitrogen and the OEC can be derived from just one peak.

Ideally, the ESEEM spectrum of an $I = 1$ nucleus coupled to an $S = 1/2$ electron spin possesses six clearly resolved peaks (Figure 1). Three of these arise from transitions between nuclear spin levels in the $m_S = +1/2$ (α) electron spin manifold while the other three features are due to nuclear spin-flip transitions in the $m_S = -1/2$ (β) manifold. In practice, however, rarely are all these transitions evident. The magnitudes of the isotropic hyperfine and nuclear Zeeman interactions are not necessarily equal, which typically leads to the appearance of just two peaks in the frequency spectrum. These are assigned to the double quantum ($\Delta m_I = 2$) transitions in each electron spin manifold, $\nu_{dq\alpha}$ and $\nu_{dq\beta}$. Accompanying these peaks could also be features at approximately half the frequencies of the ν_{dq} transitions corresponding to single quantum transitions ν_{sq}; however, these peaks are more susceptible to broadening by hyperfine anisotropy and nuclear quadrupole interaction and thus often go undetected. As the nuclear Zeeman and hyperfine interactions (HFI) become equal in magnitude, they cancel each other out in one electron spin manifold (which manifold depends on the relative signs of the interactions).[44] This leads to a coalescence of nuclear spin levels in that manifold that are split by only the nuclear quadrupole interaction (NQI). Transitions between these nominally pure quadrupole states are labeled ν_0, ν_-, and ν_+. Experimentally, this cancellation condition can be met for arbitrary hyperfine coupling by simply changing the magnitude of the applied magnetic field and performing the ESEEM experiment at the corresponding excitation frequency (maintaining a constant g value). The cancellation condition cannot be met if the magnitude of the hyperfine interaction is larger than the excitation bandwidth of the microwave pulses.

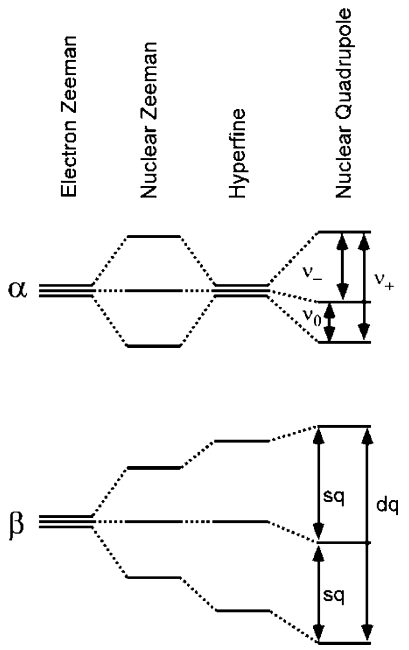

Figure 1. Energy level diagram of electron and nuclear spin levels of an $S = 1/2$, $I = 1$ spin system. As the magnitude of the applied magnetic field B_0 is increased from zero to a value where nuclear Zeeman interaction $\approx A_{eff}/2$, the spin levels in one spin manifold (α) collapse and are only split by the nuclear quadrupole interaction. This case leads to maximal modulation depth in the ESEEM spectrum.

Recently, our laboratory performed such a multifrequency (from X- to K_a-band frequencies, 9.75 to 30.76 GHz) ESEEM study of PSII-containing thylakoids isolated from spinach.[41] The K_a-band spectra possessed prominent peaks at 0.88, 1.98, 6.90, and 14.00 MHz that were well-simulated with the following magnetic parameters: $A_{iso} = 7.3$ MHz, $A_{aniso} = [+0.70\ +0.70\ -1.40]$ MHz, $e^2Qq/h = 1.98$ MHz, and $\eta = 0.84$. The results from this study afforded, for the first time, quantitative insight into the strength of the HFI of this ^{14}N nucleus to the OEC in the S_2 state. Further, it allowed for the characterization of the electric quadrupole tensor, a key parameter in assessing the electronic structure of the nitrogen atom and its chemical environment. As all observed features were fully accounted for in the simulations of the data and no combination peaks were present in the three-pulse ESEEM spectrum, we concluded that only a single ^{14}N nucleus was strongly interacting with the Mn cluster.

To further complement this new, more quantitative understanding of the proteinaceous nitrogen coordination of the OEC, we have extended these studies of spinach PSII to Q-band (34.5 GHz) and compare these findings to analogous spectra of native PSII from *Synechocystis* sp. PCC 6803 (^{14}N-PSII). We also present results from ESEEM studies of fully ^{15}N-labeled *Synechocystis* (^{15}N-PSII), which allow for a more precise determination of the nitrogen HFI as energy shifts of the nuclear spin levels due to NQI are absent. Notably, the ESEEM spectra of ^{15}N-PSII collected at K_a- and Q-band, in

dx.doi.org/10.1021/bi2010703 | *Biochemistry* 2011, 50, 7390−7404

contrast to the results obtained at X-band, are the first data to show obvious features from hyperfine-coupled ^{15}N nuclei.[38,39] To verify again that the observed isotope sensitive features arise from histidine nitrogen(s) coupling to the OEC, we have prepared ^{15}N-labeled PSII containing natural-abundance histidine (^{14}N-His/^{15}N-PSII). All these data are then compared to those of two site-directed mutants, D1-H332E and D1-D170H. Differences between these data sets are discussed in the context of recent ESEEM spectroscopic results on a D1-H332S mutant from *Thermosynechococcus elongatus*,[36] and an amino acid ligation scheme for the OEC in the S_2 state is proposed.

MATERIALS AND METHODS

Construction of Mutant Strains and Propagation of Cultures. The D1-D170H and D1-H332E mutant strains of the cyanobacterium *Synechocystis* sp. PCC 6803 have been described previously.[40,45] Each mutation was constructed in the *psbA-2* gene, and the mutation-bearing plasmid was transformed into a host strain of *Synechocystis* that lacks all three *psbA* genes and contains a hexahistidine-tag (His-tag) fused to the C-terminus of CP47. Cells were maintained on solid BG-11 media[46] containing 5 mM TES-NaOH (pH 8.0), 0.3% sodium thiosulfate, 5 mM glucose, 10 μM 3-(3,4-dichlorophenyl)-1,1-dimethylurea (DCMU), 5 μg/mL kanamycin monosulfate, and 20 μg/mL gentamycin sulfate. The DCMU, thiosulfate, and antibiotics were omitted from liquid cultures. Large-scale liquid cultures (each consisting of two or three 7 L cultures held in glass carboys) were propagated as described previously.[47] For the purification of PSII core complexes uniformly labeled with ^{15}N, liquid cultures were propagated in the presence of 10 mM $Na^{15}NO_3$ as the sole nitrogen source (98% ^{15}N enrichment, Cambridge Isotope Laboratories, Andover, MA).[37,48] For the purification of PSII core complexes containing natural abundance ^{14}N-histidine in a uniformly ^{15}N-labeled background, liquid cultures were propagated in the presence of both 240 μM L-histidine[39] and 10 mM $Na^{15}NO_3$.

Purification of PSII Core Complexes. PSII core complexes were purified under dim green light at 4 °C with Ni-NTA superflow affinity resin (Qiagen, Valentia, CA) as described previously.[49] The purification buffer consisted of 1.2 M betaine, 10% (v/v) glycerol, 50 mM MES-NaOH (pH 6.0), 20 mM $CaCl_2$, 5 mM $MgCl_2$, 50 mM histidine, 1 mM EDTA, and 0.03% (w/v) *n*-dodecyl β-D-maltoside. The purified PSII core complexes were concentrated to ≈9 mg of Chl/mL by ultrafiltration, frozen in liquid N_2, and stored at −80 °C. DCMU was added to 1 mM to samples of D1-H332E mutant. No electron acceptor was added to any PSII samples. Subsequently, the concentrated PSII core complexes were loaded into 2.5 mm diameter and 1.5 mm diameter quartz tubes for study by K_a- and Q-band EPR spectroscopy, respectively. To verify the integrity of the mutant PSII core complexes, an aliquot of each large-scale culture was set aside, and the sequence of the relevant domains of the D1 polypeptide was obtained after PCR amplification of genomic DNA.[50] No trace of the wild-type codon was detected in any of the mutant cultures.

PSII from spinach (BBY) was purified according to the method of Berthold, Babcock, and Yocum[51] modified to remove adventitiously bound Mn(II).[52,53]

Hydrolysis, Derivatization, and Mass Analysis of Histidine. The mass distribution of histidine residues in the ^{14}N-His/^{15}N-PSII preparation was assessed by mass spectrometry. The effluent from the Ni-NTA affinity column (consisting of thylakoid proteins other than PSII) was adsorbed onto a Pharmacia Q-Sepharose fast flow ion-exchange column, washed with 50 mM MES-NaOH (pH 6.0) 0.03% DM to remove excess *n*-dodecyl β-D-maltoside and other contaminants, and then eluted with 50 mM MES-NaOH (pH 6.0), 0.03% *n*-dodecyl β-D-maltoside, 0.5 M NaCl. The effluent was then passed through a Pharmacia HR26/10 desalting column to remove NaCl and concentrated to about 10 mg of Chl/mL with Centricon-100 concentrators.

For hydrolysis, an aliquot of concentrated ^{14}N-His/^{15}N-protein solution was precipitated with 0.700 mL of 95% acetone (HPLC grade) followed by 30 s of vortexing. The sample was incubated for 90 min in a −20 °C freezer prior to centrifugation at 14000*g* for 10 min at 4 °C. The supernatant was removed, and the remaining pellet was dried under gaseous N_2 for 3 h. The dried pellet was then transferred to a glass vial, flushed with N_2 gas, and 0.30 mL of 6 M HCl was added. Following acidification, the sample was then sealed and placed in an oil bath at 120 °C for 24 h. Once cooled to room temperature, the residual solvent was evaporated with flowing N_2 gas. The hydrolyzed sample was then derivatized with *tert*-butyl dimethylsilylate as previously described.[54] Gas chromatography to mass spectrometry (GC/MS) spectroscopic analysis was performed at the UC Davis Proteomics/Genomics Center.

EPR Spectroscopy. The K_a-band (30.5−31.5 GHz) experiments were performed using a laboratory-built pulse EPR spectrometer and ESEEM probe that have been described previously.[55] Low-temperature operation was achieved using a Janis Research Co. (Wilmington, MA) SuperVariTemp cryostat in conjunction with a Lakeshore Cryotronics (Westerville, OH) temperature controller. Q-band (34.5 GHz) experiments were performed with a Bruker Elexsys E580 pulse EPR spectrometer (Bruker BioSpin, Billerica, MA) fitted with a SuperQ-FT multifrequency extension and using an EN 5107D2 resonator. Cryogenic temperatures were achieved and maintained with an Oxford CF-935 cryostat and Oxford ITC temperature controller.

All presented EPR spectra were generated by subtracting the spectrum of dark-adapted PSII particles from that obtained following 8 min of continuous illumination (using a Sylvania ELH 300 W halogen−tungsten lamp, color temperature = 3350 K) at 200 K. D1-H332E samples were illuminated at 195 K (ice/water) for 1 min as described previously.[34,40] These light-*minus*-dark spectra ideally contain only features associated with the OEC trapped in the S_2 state. However, the redox-active tyrosine Y_D found in the D2 polypeptide of PSII, the Fe/Q_A site on the acceptor side of PSII, and cytochromes bound in nearby proteins all have EPR signals that can change upon illumination.[21] Therefore, two-pulse ($\pi/2-\tau-\pi-\tau-$echo) and three-pulse ($\pi/2-\tau-\pi/2-T-\pi/2-\tau-$echo) ESEEM experiments were performed at five magnetic field positions across the EPR envelope of the MLS. The signal from $Y_D^{\bullet}$ is centered at g = 2 and only 4 mT wide. The signals from oxidized cytochrome and Fe(II)/Q_A^- are broader than the MLS (the photoinduced Fe(II)/Q_A^- signal appears at g = 1.90 and 1.64 or g = 1.82 and 1.67 depending on the presence or absence of CO_2/HCO_3^-),[21] though anisotropic and have intensity maxima on the low-field and high-field sides, respectively, of

the g = 2 region of the spectrum. Thus, only peaks from the OEC in the S_2 state should appear in all five spectra. Furthermore, the Fe(II)/Q_A^- spin system is known to relax very quickly and does not contribute to ESE EPR spectra collected at 4.5 K.[56] Indeed, the ESEEM features analyzed below are present in all five resonant field positions and appear at frequencies that are different due solely to the change in the nuclear Zeeman interaction as B_0 changes. Three-pulse ESEEM spectra were acquired using multiple τ values to ensure that no spectral features were suppressed. Other relevant instrument settings are given in the corresponding figure captions. Frequencies contributing to observed modulation patterns were visualized using cosine-Fourier transforms backfilled with only the two highest frequency components of the spectrum.[57] Spectral simulations were performed with the Matlab 7.5.0.342 (R2007b) software package (The Mathworks Inc., Natick, MA) using the EasySpin 3.1.5 toolbox.[58,59]

RESULTS

Two-Pulse Electron Spin-Echo Detected (ESE) EPR. The K_a-band two-pulse ESE field-swept EPR spectrum for each PSII sample described in the Materials and Methods section is presented in Figure 2. The spectra are, for comparison, plotted versus the effective g-values instead of B_0, to account for the slightly different microwave frequencies at which they were acquired. For clarity, the signal from $Y_D^\bullet$ was removed from each trace. Excepting the data of the D1-H332E mutant, all the EPR spectra possess partially resolved ^{55}Mn hyperfine couplings.

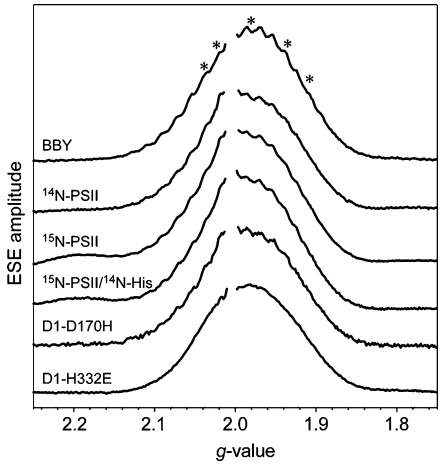

Figure 2. K_a-band two-pulse ESE field-swept light-*minus*-dark spectra of different preparations of PSII. (A) Ethanol-treated PSII from spinach (BBY) and from *Synechocystis* (B) ^{14}N-PSII, (C) ^{15}N-PSII, (D) ^{15}N-PSII/^{14}N-His, (E) D1-D170H, and (F) D1-H332E. The asterisks indicate the positions (g factors kept constant) at which two- and three-pulse ESEEM experiments were performed. All K_a-band data presented in Figures 3–6 were acquired at g = 1.98. Microwave excitation frequency: (A–C) ν_{MW} = 30.757 GHz, (D) ν_{MW} = 30.783 GHz, (E) ν_{MW} = 30.847, and (F) ν_{MW} = 30.562 GHz. Additional instrument settings: $\pi/2$ = 30 ns, τ = 220 ns, ΔB_0 = 1 mT, repetition time = 5 ms, T = 4.5 K.

The spectrum of ethanol-treated PSII from spinach (BBY) has a symmetric, Gaussian line shape centered at g = 1.98, while the *Synechocystis* samples have spectra that have a slight asymmetry with greater intensity evident on the low field side of the $Y_D^\bullet$ signal. This difference could be due to the contribution from of a small amount of photooxidized cytochrome (g values = [2.98, 2.25, 1.53]).[60] All high(er)-field EPR studies (Q-band and W-band (94 GHz)) of plant[61] and cyanobacterial[62,63] PSII frozen solutions and single crystals have shown that principal g values of the OEC in the S_2 state are very nearly axial (e.g., g = [1.988, 1.981, 1.965] for PSII from *Thermosynechococcus vulcanus*[63]). Therefore, the observed asymmetry in the EPR spectrum of some of the *Synechocystis* samples cannot be attributed to changes in g anisotropy of the S_2 signal between plant and cyanobacterial PSII.

The ESE–EPR spectra of wild-type PSII in Figure 2 were scaled according to the nominal concentration of OEC (inferred on the basis of spectrophotometrically determined chlorophyll concentration). The actual integrated areas of the signals of PSII core particles from *Synechocystis* are each within 10–15% of the ethanol-treated samples from spinach, suggesting that the respective peptides are fully loaded with OEC and able to advance to at least the S_2 state.

The asterisks in Figure 2 denote the g values at which two- and three-pulse ESEEM experiments were performed. All spectra shown in subsequent figures were acquired in resonance with the magnetic field position corresponding to g = 1.98. As described in the Materials and Methods section, all features observed in the presented frequency spectra were seen at all field positions examined.

Two-Pulse and Three-Pulse ESEEM. *Natural Abundance PSII (BBY and ^{14}N-PSII).* The light-*minus*-dark K_a-band two-pulse ESEEM spectra of BBY, ^{14}N-PSII, and ^{15}N-PSII are shown in Figure S2. The corresponding frequency spectra achieved by cosine-backfilled Fourier transform are presented at the bottom of Figure S2. For each species, time-domain spectra acquired at K_a- and Q-band (see Supporting Information for Q-band data) excitation frequencies are quite similar, with both data sets showing deep modulation. The K_a-band spectrum of BBY (B_0 = 1107.9 mT) is the same as that published previously and is shown again here for comparison to that of *Synechocystis* PSII.[41] The BBY two-pulse ESEEM spectrum has peaks at 2.09, 6.9, and 14.2 MHz that are nearly identical to features found in the ^{14}N-PSII spectrum (B_0 = 1107.9 mT) at 2.11, 6.9, and 14.3 MHz. Also present in the ^{14}N-PSII spectrum are two features at 4.6 and 9.4 MHz with negative intensity that flank the positive peak at 6.9 MHz. Such negative intensity features are common in two-pulse ESEEM data and indicate that the corresponding peaks arise from combination frequencies (sum and difference) of the 2.11 and 6.9 MHz transitions. The lifetime of the spin-echo in a two-pulse ESEEM experiment is limited by the phase memory time, which, for the OEC at 4.5 K, is relatively short ($T_m \approx 0.5$ μs). As a result, low-frequency modulations (<2 MHz) are poorly resolved.

Light-*minus*-dark three-pulse ESEEM spectra of BBY, ^{14}N-PSII, and ^{15}N-PSII are shown in Figure 3. In contrast to the two-pulse ESEEM data, the intensity of the three-pulse ESEEM stimulated echo is not limited by phase memory but rather by spin–lattice relaxation (T_1), which is much longer in this case. Thus, modulations can persist for much longer making low-frequency modulations easier to detect and the higher-frequency features narrow compared to corresponding features in the two-pulse ESEEM spectrum. Additionally, combination peaks do not appear in three-pulse ESEEM spectra unless nearly equivalent hyperfine-coupled nuclei are present. Similar

dx.doi.org/10.1021/bi2010703 | *Biochemistry* 2011, 50, 7390–7404

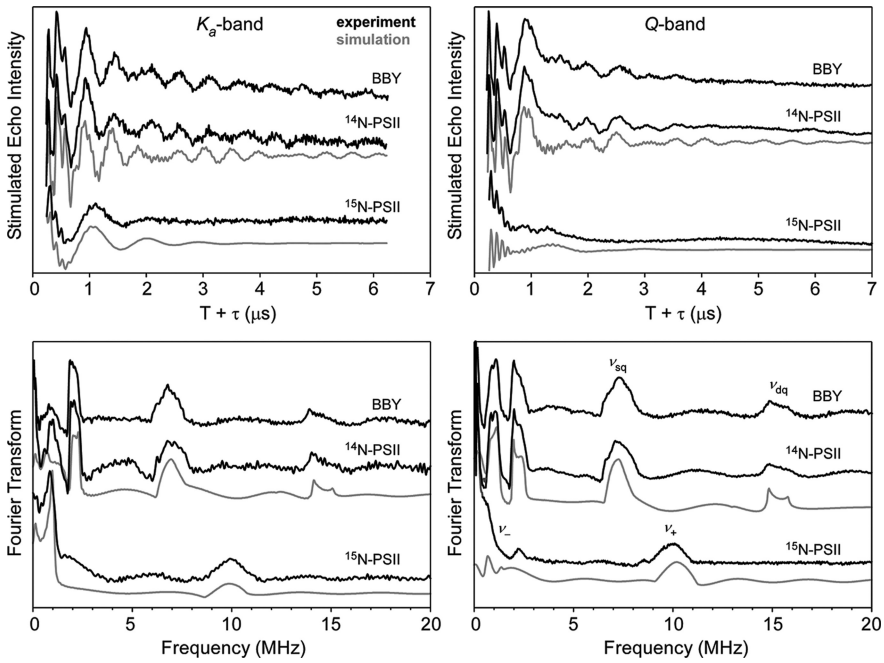

Figure 3. Time-domain (top) and corresponding cosine-backfilled Fourier transformed (bottom) K_a-band (left) and Q-band (right) three-pulse ESEEM spectra of BBY and ^{14}N-PSII and ^{15}N-PSII from *Synechocystis*. K_a-band instrument settings ν_{MW} = 30.757 GHz, B_0 = 1.1079 T, $\pi/2$ = 15 ns, τ = 170 ns, ΔT = 15 ns, repetition time = 5 ms, and T = 4.5 K. Q-band instrument settings for *Synechocystis* spectra: ν_{MW} = 33.927 GHz, B_0 = 1.2229 T, $\pi/2$ = 16 ns, τ = 172 ns, ΔT = 16 ns, repetition time = 5 ms, T = 4.5 K. For spinach PSII spectra: ν_{MW} = 33.888 GHz, B_0 = 1.2225 T, $\pi/2$ = 16 ns, τ = 172 ns, ΔT = 16 ns, repetition time = 5 ms, and T = 4.5 K Spectral simulations were performed using the parameters given in Table 1.

sets of peaks appear in both the BBY and ^{14}N-PSII K_a-band three-pulse ESEEM spectra at 0.93, 2.01, 6.9, and 14.0 MHz and at 0.97, 2.00, 6.9, and 14.0 MHz, respectively (Figure 3, left). No additional spectral features are present in respective Q-band three-pulse ESEEM spectra (Figure 3, right). However, the two highest frequency peaks in the K_a-band spectra have shifted higher in Q-band spectra—Δ = 0.34 and 0.70 MHz—due to an increase in the ^{14}N nuclear Zeeman field. These shifts are consistent with the features being assigned to the ν_{sq} and ν_{dq} transitions, respectively. That the other, lower-frequency features at approximately 1 and 2 MHz do not significantly change frequency with increasing B_0 is diagnostic of their arising from nuclear transitions between nearly pure quadrupole states.

Uniformly ^{15}N-Labeled PSII (^{15}N-PSII). The K_a- and Q-band ESEEM spectra of PSII from *Synechocystis* grown with $^{15}NO_3^-$ as the sole nitrogen source are compared to those of BBY and ^{14}N-PSII in Figure 3 and Figure S2. The K_a-band two-pulse ESEEM spectrum of ^{15}N-PSII lacks all features found in the natural abundance isotopologue spectra (Figure S2). Instead, a strong peak appears at 9.7 MHz. Possible combination peaks (negative features) at 8.6 and 10.8 MHz are present as well as a narrow feature at 0.9 MHz. The two-pulse ESEEM spectrum for ^{15}N-PSII was very sensitive to background correction (cf. traces in Figure S3). For the Q-band data, a strong feature is observed at 10.30 MHz with a positive shoulder centered at 9.4 MHz. Two negative features appear at 7.75 and 11.27 MHz, and a broad, less intense, positive feature is centered at ≈18 MHz.

The corresponding three-pulse ESEEM spectra are more illuminating. A low-frequency modulation is now evident in the spectra at both excitation frequencies (Figure 3). The K_a-band spectrum has a narrow, intense feature at 0.85 and a broader peak at 9.9 MHz. These features are assigned to the ν_a and ν_b ^{15}N nuclear spin-flip transitions in the two electron spin manifolds. That the latter peak appears at roughly twice the ^{15}N Larmor frequency at B_0 = 1108 mT ($\nu_L(^{15}N)$ = 4.78 MHz) indicates that the corresponding ^{15}N nucleus is experiencing near-cancellation conditions. Thus, the isotropic (A_{iso}) and dipolar (A_{dip}) contributions to the hyperfine matrix can be estimated directly from the frequencies of the two peaks seen Figure 3 (0.85 and 9.9 MHz) using the following relations: $\nu_a \approx {}^3/_4 A_{dip}$ and $\nu_b \approx A_{iso} + A_{dip}/2$.[64] We estimate $A_{iso}(^{15}N)$ = 9−10 MHz and $A_{dip}(^{15}N)$ = 0.85−1.2 MHz. Peaks in the Q-band spectrum are more structured yet broader than those in the K_a-band spectrum, signaling a departure from cancellation conditions (i.e., $\nu_L(^{15}N)$ is no longer approximately equal to $A_{eff}/2$).

Additional, though small, spectral features at 2.25 and 8.45 MHz are apparent in Q-band three-pulse ESEEM light-*minus*-dark spectra. These features are centered at the ^{15}N Larmor frequency of 5.28 MHz (at 1222.9 mT) and split by ≈6 MHz. No corresponding peaks are obvious in any of the K_a-band ESEEM spectra of ^{15}N-PSII. While these features may arise from an additional ^{15}N nucleus that is hyperfine coupled to the OEC, it is more likely that they are from the four heme nitrogens of cytochrome b_{559} (Cyt b_{559}). Indeed, these peaks are also seen in the spectrum of dark-adapted PSII, and the simulated ESEEM spectrum generated using reported ^{15}N HFI parameters for Cyt b_{559} perfectly reproduces the frequencies observed here (see Supporting Information).[60] The intensity of the Cyt b_{559} EPR spectrum in cyanobacterial PSII preparations is known to be sensitive to light.[21] This could lead to incomplete subtraction of the Cyt b_{559} signal and allow nuclei coupled to the low-spin heme to be a minor contribution to the light-*minus*-dark ESEEM spectra.

ESEEM Simulations. In both the spectra of ^{14}N-PSII and ^{15}N-PSII from *Synechocystis*, all features are assumed to arise

dx.doi.org/10.1021/bi2010703 | *Biochemistry* 2011, 50, 7390−7404

from the coupling of a single nitrogen nucleus to the $S = 1/2$ electron spin of the OEC poised in the S_2 state. The precise magnitude of this magnetic coupling reports on not only the electronic structure of the nitrogen atom but also the nature of the coordinating Mn ion—namely its oxidation state—as well. Beginning with the ^{15}N hyperfine values estimated from the K_a-band ESEEM spectra above, we have simultaneously fit the ^{15}N- and ^{14}N-PSII ESEEM time traces obtained at both K_a- and Q-band excitation frequencies using a least-squares optimization routine implemented in EasySpin.[58,59] Spectra acquired using other values of τ were also used to constrain the simulation.

These best-fit three-pulse simulations were achieved with the following spin Hamiltonian parameters for the coupled ^{14}N center (the parameters for the ^{15}N-PSII ESEEM simulations are given simply by scaling the hyperfine values determined for ^{14}N by the ratio of the respective nuclear gyromagnetic ratios; $\gamma(^{15}N)/\gamma(^{14}N) = -1.4028$): $A_{iso} = 6.95$ MHz, $A_{aniso} = [0.20\ 1.30\ -1.50]$ MHz, $e^2Qq/h = -1.98$ MHz, and $\eta = 0.815$. The signs of the contributing terms to the hyperfine interaction are only relative. The sign of e^2Qq/h is assumed to be negative based on electron nuclear double resonance (ENDOR) data of other metal-coordinated imidazoles.[65]

The time-domain ESEEM data and corresponding Fourier transforms for BBY and ^{14}N-PSII are essentially identical as is shown in Figure 3. As a result, the magnetic parameters determined here for *Synechocystis* PSII are very similar to those determined for the nitrogen coupled to the OEC in spinach PSII.[41] The modest differences in the nitrogen hyperfine tensor—a 0.35 MHz reduction in A_{iso} and an increase in hyperfine anisotropy—were required to properly simulate the ESEEM spectrum of ^{15}N-PSII, an isotopologue that was not available for our earlier study on BBY. We therefore argue that the strength of the ^{14}N hyperfine interaction with the unpaired electrons on the OEC in the S_2 state is virtually identical between spinach and *Synechocystis* PSII.

Natural Abundance Histidine in ^{15}N-PSII (^{14}N-His/^{15}N-PSII). To assign the nitrogen-isotope-sensitive features found in the above ESEEM data, we have also examined samples of uniformly ^{15}N-labeled PSII that contain natural abundance ^{14}N-histidine (^{14}N-His/^{15}N-PSII). These data should allow for facile distinction between spectroscopic features from nitrogens in histidine and those from other sources such as the polypeptide amide backbone or other nitrogen-containing amino acid side chains (e.g., lysine, glutamine, arginine, etc.).

The K_a-band ESEEM spectrum of ^{14}N-His/^{15}N-PSII is presented in Figure 4A and has features at 1.0, 2.0, 7.0, 9.9, and 14.0 MHz. Upon comparison of this spectrum to analogous data of ^{14}N-PSII and ^{15}N-PSII, it is clear that ^{14}N-His/^{15}N-PSII has spectral features common to both isotopically pure samples. Mass spectrometric analysis of the TBS-derivatized hydrolyzed ^{14}N-His/^{15}N-PSII shows that ≈60% of histidine residues in the sample remain ^{15}N-labeled as indicated by the peak at 443 m/z in Figure 4B and the remaining 40% are ^{14}N-labeled (peak at 440 m/z). Therefore, simulation of the three-pulse ESEEM spectrum of ^{14}N-His/^{15}N-PSII (Figure 4A) requires a combination of the ^{14}N and ^{15}N computed signals from above (Figure 3). The two contributing time-domain signals were each generated using the magnetic parameters given in Table 1. The resulting ^{14}N and ^{15}N spectra were scaled by the factors 0.4 and 0.6, respectively, and then added together. The resultant simulated spectrum models the experimental data extremely well. Though this degree of isotope contamination is quite high given that previous similar experiments showed the histidine isotopologue heterogeneity to be ≈15%,[39,66,67] the agreement of the GS/MS results with the observed ratio in the ^{14}N-His/^{15}N-PSII ESEEM spectrum confirms that all features arise from histidine nitrogen that is strongly interacting with the OEC.

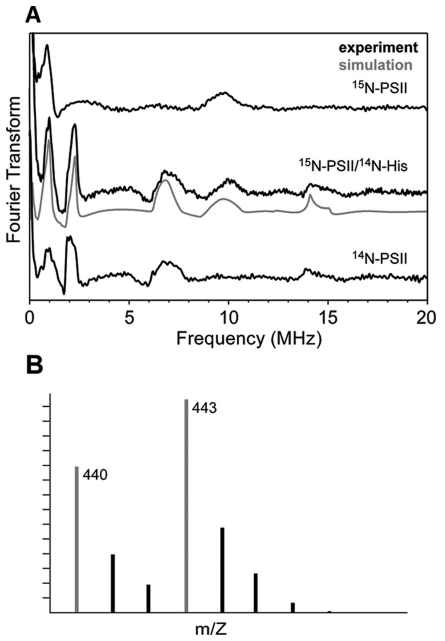

Figure 4. (A) Cosine-backfilled Fourier transformed K_a-band three-pulse ESEEM spectrum of ^{15}N-PSII/^{14}N-His (center) compared to those for ^{14}N-PSII (top) and ^{15}N-PSII (bottom). The ^{14}N-PSII and ^{15}N-PSII spectra are the same as those presented in Figure 3, bottom left. Acquisition of the ^{15}N-PSII/^{14}N-His spectrum employed the following instrument settings: $\nu_{MW} = 30.837$ GHz, $B_0 = 1.1118$ T, $\pi/2 = 10$ ns, $\Delta T = 15$ ns, repetition time = 5 ms, $T = 4.5$ K and is the sum of spectra obtained using three different values for $\tau = 170$, 200, and 210 ns. (B) GC/MS mass spectrum of the TBS-derivatized hydrolyzed ^{15}N-PSII/^{14}N-His.

Site-Directed Mutants. To identify amino acids that could be coordinating to the OEC, we have examined the EPR spectra of two site-directed PSII mutants, D1-H332E and D1-D170H. On the basis of mutagenesis and crystallographic studies, both D1-His332 and D1-Asp170 have been suggested as ligands to the Mn cluster.[4] The ESE EPR spectra of the D1-H332E and D1-D170H mutants (Figure 2) are reduced in intensity by 65% and 45%, respectively, compared to that of ^{14}N-PSII. Previously, EPR spectra of D1-H332E PSII have been shown to have only 60% of the MLS found for wild-type*.[34] Notably, the K_a-band D1-H332E spectrum lacks ^{55}Mn hyperfine features that are present in all other data. The S_2 state of this mutant is known to have a narrower X-band EPR spectrum with ^{55}Mn hyperfine lines that are split by much less than is observed for the wild-type* enzyme. A similarly altered MLS has also been found for ammonia-treated[68] and strontium-substituted[69] PSII preparations.

The ESE EPR spectrum of D1-D170H, on the other hand, is very similar to that of ^{14}N-PSII. Its reduced intensity is correlated with a decrease in oxygen evolution activity (60% that of wild-type*).[70] One cause of these effects could be a decrease in the success of OEC photoassembly during which

dx.doi.org/10.1021/bi2010703 | *Biochemistry* 2011, 50, 7390–7404

Table 1. Magnetic Coupling Parameters for Nitrogens Bound to Biological Mn Clusters

species	A_{iso} (MHz)	A_{aniso} (MHz)	e^2Qq/h (MHz)	η	ref
^{14}N-PSII (*Synech.*)[a]	6.95	0.2 1.3 −1.5	1.98	0.82	this work
^{15}N-PSII (*Synech.*)	−9.75	−0.3 −1.8 2.1	n.a.	n.a.	this work
PSII (BBY)	7.3	+0.5 +0.5 −1.0	1.98	0.84	41
superoxidized MnCat (*L. plantarum*)	+2.67	+0.41 +0.16 −0.57	2.25	0.58	75
	−5.75	−0.2 −0.6 +0.8	2.01	0.79	
superoxidized MnCat(*T. thermophilus*)	+2.28	+0.42 +0.28 −0.70	2.29	0.50	75
	−5.2	−0.3 −0.7 +1.0	2.25	0.65	

[a]Euler rotation angles between the hyperfine and nuclear quadrupole tenors $[\alpha, \beta, \gamma] = [-30, 0, 40]°$.

D1-Asp170 has been directly implicated as a participant.[70−74] The K_a- and Q-band ESEEM data of D1-D170H PSII show deep modulation patterns that are identical to those observed for ^{14}N-PSII. Additional three-pulse ESEEM data sets for D1-D170H acquired using other τ values and, at other magnetic field positions, found no differences compared to analogous data of ^{14}N-PSII.

Earlier ESEEM studies performed at X-band showed that a nitrogen isotope sensitive feature at ≈5 MHz is greatly affected by the D1-H332E mutation (see Figure S1).[38−40] The K_a-band three-pulse ESEEM data of D1-H332E PSII presented here are devoid of any modulations (Figure 5, top) and thus give rise to no peaks in the Fourier transform (Figure 5, bottom; see also Figure S8).

DISCUSSION

Quantitative Analysis of Nitrogen Coupling to OEC.

Simultaneous fitting of the K_a- and Q-band ESEEM spectra of ^{14}N-PSII and ^{15}N-PSII from *Synechocystis* sp. PCC 6803 acquired at multiple resonant field positions yielded precise magnetic parameters for a single nitrogen nucleus coupled to the Mn cluster in the S_2 state. These parameters—A_{iso} = 6.95 MHz, A_{aniso} = [0.20 1.30 −1.50] MHz, e^2Qq/h = 1.98 MHz, and η = 0.815—are reminiscent of those found for the imidazole nitrogen from histidine that is coordinated to the Mn(III) ion of the dimanganese-containing catalase (MnCat) poised in the Mn(III)Mn(IV) state.[75] These features must arise from a histidine imidazole group because the ESEEM spectrum of ^{15}N-PSII containing ^{14}N-His as the sole source of ^{14}N possesses features found in the spectrum of the isotopically pure ^{14}N-PSII (see Figure 4).

The effective hyperfine interaction measured here is dominated by a large isotropic contribution A_{iso}. The value of A_{iso} depends on (i) the degree of overlap between the nitrogen nucleus and the Mn-centered orbitals containing unpaired electrons (Fermi contact, f_s), (ii) the hybridization of the nitrogen 3s−2p^n orbitals, and (iii) the projection factor c for the coordinating Mn ion (*vide infra*).

$A_{iso}(^{14}N)$ for PSII is larger than all other known Mn−N effective hyperfine couplings except for those resulting from a Mn−N bonding vector that is coincident with a lobe of a singly occupied metal-centered 3d orbital.[75−77] For example, broken-symmetry density functional theory (BS DFT) computations on mixed-valence Mn(III)Mn(IV) dimers have shown that when the nitrogen nucleus lies along the local z-axis of the Mn(III) ion, there is a strong hyperfine interaction with the half-occupied $3d_{z^2}$ orbital.[78] ENDOR studies of such compounds have detected a ^{14}N HFI on the order of 9−13 MHz

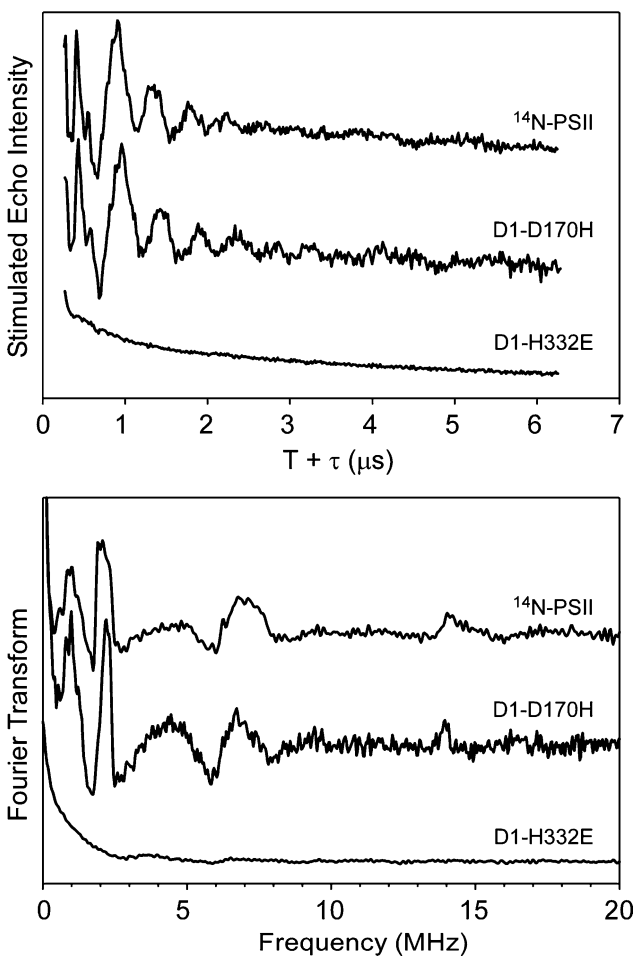

Figure 5. Time-domain (top) and corresponding cosine-backfilled Fourier transformed (bottom) Q-band three-pulse ESEEM spectra of D1-H332E and D1-D170H PSII compared to those of ^{14}N-PSII. The ^{14}N-PSII spectrum is the same as that presented in Figure 3, bottom right. Instrument settings for D1-D170H data collection: ν_{MW} = 30.783 GHz, B_0 = 1.1098 T, $\pi/2$ = 10 ns, τ = 200 ns, ΔT = 15 ns, repetition time = 5 ms, T = 4.5 K. For D1-H332E data collection: ν_{MW} = 30.562 GHz, B_0 = 1.1063 T, $\pi/2$ = 10 ns, τ = 210 ns, ΔT = 15 ns, repetition time = 5 ms, T = 5.0 K.

that is ascribed to such a coupling mode.[76,79] Also contributing to this large effective HFI is the projection factor of c = +2 for the coordinating Mn(III) ion in the dimer.[80] These projection factors are computed by determining the expectation value of the local electron spin projected onto the total electron spin of the molecule.[81] The Fermi contact can

dx.doi.org/10.1021/bi2010703 | *Biochemistry* 2011, 50, 7390−7404

then be calculated using

$$f_{2s} = 2S\frac{A_{iso}/c}{a^{\circ}}$$

where a° is the HFI of one electron spin in a ^{14}N 2s orbital (+1811 MHz)[82] and S is the local electron spin of the coordinating ion, 2 in the case of Mn(III). For Mn(III)Mn(IV) MnCat from *Lactobacillus plantarum*, we found that the ^{14}N atom bound to the Mn(III) ion had an unpaired spin in the 2s orbital (f_{2s}) equal to 0.64%.[75]

That the OEC is composed of exchange-coupled paramagnetic ions leads to a ladder of possible spin states—the lowest of which has a total spin of $S = 1/2$, for the S_2 state. Results from pulse EPR inversion recovery studies established a range of values for the energy gap between the ground and first-excited spin state manifolds (24−36.5 cm^{-1}, depending on the origin of the and method of preparation of the PSII).[29,30,83] Using this value combined with data from ^{55}Mn ENDOR spectroscopic studies,[27,29,30] we and others have proposed a scheme for the exchange coupling of the four Mn centers and assigned formal oxidation states. We believe that in the S_2 state the lone Mn(III) ion is part of the [Mn_3Ca] cuboidal/pyramidal cluster that is weakly exchange coupled to Mn_D (Figure 6). The isotropic projection factors computed by Peloquin et al.[27] for this arrangement are $c_{Mn(III)} = 1.77$ and $c_{Mn(IV)}$ ranges from 1.00 to 1.27. We note that the projection factors determined in refs 29 and 30 are not substantially different from these values. If histidine is coordinated to the Mn(III) ion, the resulting $f_{2s}(^{14}N)$ is 0.87%. If instead the imidazole is bound to one of the remaining Mn(IV) ions, this would correspond to a range of $f_{2s}(^{14}N)$ is 0.91−1.15%.

That the ^{14}N Fermi contact computed above is so much larger than those measured for the equatorially liganded histidines in MnCat suggests that histidine is bound along an axis that contains a lobe of a half-occupied metal-centered orbital. Such a binding geometry seems unlikely for a high-spin d^3 Mn(IV) ion as disruption of a pseudo-octahedral ligand field would lead to a significant loss of ligand field stabilization energy. Therefore, we prefer the description of the bonding partner to histidine as being a Mn(III) ion. In this case, the larger projection factor for a Mn(III) bound nitrogen rationalizes the observed large ^{14}N HFI.

The nuclear quadrupole coupling parameters e^2Qq/h and η reported above are at the extreme of the range of those found previously for d^{10} M(II)-coordinated imidazoles,[84] though almost identical to that found for the histidine bound to the Mn(III) ion in superoxidized MnCat, $e^2Qq/h = 2.01$ MHz (Table 1).[75] The largest part of the electric field gradient at the nitrogen nucleus (q) is expected to coincide with the direction of the nitrogen lone pair—presumably lying along the Mn−N bonding axis. Though, in the absence of ESEEM data on oriented single crystals, we cannot be certain of this assignment. The magnitude of e^2Qq/h measured for ^{14}N-PSII indicates significant charge donation from the nitrogen lone pair to the Mn center, reducing its population from 2.00 to ≈1.65 electrons. This depopulation is driven by the Lewis acidity and high formal charge of the coordinating metal as well as the σ-donor strength of the histidine ligand.

Earlier studies have shown that the S_2 MLS for BBY preparations has nearly identical spectral and spin-relaxation properties as those found for PSII derived from cyanobacteria.[29,30,62,63,85]

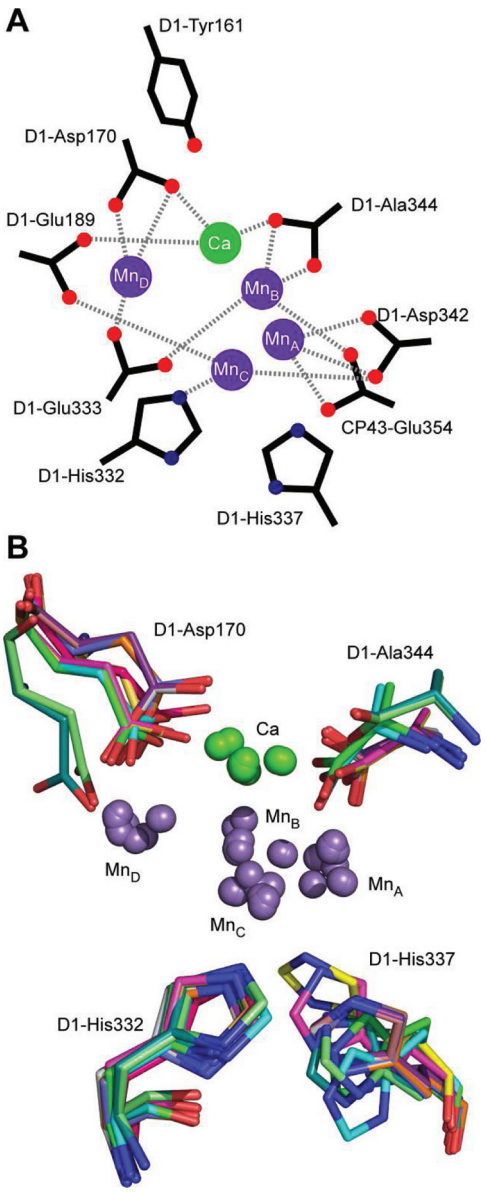

Figure 6. (A) Schematic representation of OEC including several possible liganding amino acids residues. (B) Superposition of [Mn_4Ca] clusters and D1-Asp170, D1-His332, and D1-His337 from all available PDB-deposited X-ray crystallographic structures.

As their magnetic properties are so similar, one can presume that structures of the respective OECs are also similar. Thus, it not surprising that the magnetic parameters for the histidine nitrogen determined in this study of *Synechocystis* PSII are comparable to those found in our earlier K_a-band ESEEM study of PSII from spinach (cf. Table 1 and Figures 3 and 4).[41] As such, we expect that the origin of the nitrogen coupling is the same for each protein.

Identification of Proteinaceous Ligands to the OEC.

Despite the advent of numerous X-ray structures, the identity of the proteinaceous ligands to the OEC in each of the five S-states remains somewhat controversial. Analysis of these PSII crystal structure data in conjunction with results from spectroscopic and biochemical studies of site-directed mutants suggest a number of possible ligands (see Figure 6A). However, the X-ray beam-induced reduction of the Mn sites to the 2+

dx.doi.org/10.1021/bi2010703 | *Biochemistry* 2011, 50, 7390−7404

oxidation state leads to changes in the metal coordination environment.[86,87] One possible manifestation of this effect is illustrated in Figure 6B which compares the positions of D1-Asp170, D1-His332, D1-His337, D1-Ala344, and the five metal ions of the OEC determined in each of the crystal structures of PSII from *T. elongatus* and *T. vulcanus* (PDB entries 1S5L, 1W5C, 2AXT, 3A0B, 3A0H, 3BZ1, 3BZ2, and 3KZI).[5−13] While the position of D1-His332 is conserved with its imidazole in close proximity to Mn_C, D1-Asp170 and D1-His337 seem to sample a wide conformational space. Thus, we must rely on results from nondestructive spectroscopic techniques such as Fourier transform infrared (FTIR) difference and EPR to assess the native coordination environment of the OEC.

A recent Q-band (35 GHz) ENDOR study of *Synechocystis* PSII for which all alanine residues were ^{13}C-labeled at the carbonyl carbon position showed conclusively that D1-Ala344 is coordinated to Mn with $A_{iso} \approx 1.0-1.2$ MHz.[35] These findings corroborated earlier results from FTIR difference spectra which indicated that D1-Ala344 is bound to a Mn ion that undergoes a change in oxidation state upon advancement from S_1 to S_2.[49,66,88] Analogous ENDOR data on uniformly ^{13}C-labeled PSII particles indicated that several other carbon-containing moieties are magnetically coupled to the OEC in the S_2 state. However, the assigning of these additional spectral features to specific amino acid ligands is ongoing.

One oft-posited carboxylate ligand candidate is the aspartate residue at position 170 in the D1-polypeptide.[45,50,70−73,89−92] During photoassembly, D1-Asp170 has been shown to be of great importance in the binding of the first equivalent of Mn(II) ion to the Mn-depleted PSII protein.[72−74,91] This ion is then photo-oxidized to Mn(III) by the same electron transfer machinery responsible for water oxidation as the first step in generating the active OEC. Several of the X-ray structures show D1-Asp170 as being closest to Mn_D (Figure 6B).

As it was not possible to site-specifically introduce magnetic nuclei (e.g., ^{13}C (I = 1/2) or ^{17}O (I = 5/2)) into the carboxylate side-chain of D1-Asp170, we instead specifically mutated into this position a histidine to use its two ^{14}N atoms (I = 1) of the imidazole side chain to probe possible magnetic couplings with the OEC. The effects of the D1-D170H mutation were first evaluated by FTIR difference studies.[45,50,93] These spectra showed no changes compared to those of the wild-type* enzyme in the 1000−1800 cm^{-1} region, implying that the carboxylate of aspartate is not bound to a Mn center that is oxidized from S_0 to S_3. It is noteworthy, however, that computational studies of OEC models have suggested carboxylate vibrational modes would be insensitive to metal ion oxidation if the corresponding change in charge is delocalized over the entire OEC.[94]

Earlier X-band[70] and the present K_a- and Q-band ESEEM spectra of the D1-D170H mutant show no new features compared to analogous spectra of the wild-type* enzyme (see Figure 5). On the basis of analogy to our EPR studies of MnCat,[75] if D1-His170 were coordinated to a Mn(IV) ion, we would have expected to see evidence of this coupling in the X-band ESEEM spectrum. If it were instead bound equatorially to a Mn(III) ion, we should have seen features in the K_a- and Q-band ESEEM spectra. That we see no features at all these excitation frequencies may suggest that the D1-His170 imidazole is not a ligand to Mn. However, given the presence of other magnetic nuclei that are coupled to the OEC and are strongly modulating (e.g., ^{14}N from either D1-His332 or D1-His337, see below), modulations from a weakly coupled D1-His170 could be lost due to cross-suppression effects.[95] Alternatively, the hyperfine coupling could be sufficiently anisotropic as to broaden the corresponding ESEEM features beyond detection. Another possibility is that D1-His170 samples a wide conformational space when the OEC is poised in the S_2 state as implied by the varied positions D1-Asp170 adopts in X-ray crystallographic results (Figure 6). This would lead to inhomogeneous broadening of any corresponding ESEEM features. Finally, the magnitude of hyperfine coupling could be so large as to make the energy of nuclear spin-flip transitions—necessary to observe the ESEEM effect—beyond the excitation bandwidth of the microwave pulses. This last possibility, though, is unlikely. X-band CW EPR spectra of WT* and D1-D170H samples poised in both the S_1 and S_2 states have essentially identical line widths.[70] An earlier comparison of PSII from spinach grown hydroponically on ^{14}N-nitrate and ^{15}N-nitrate showed no discernible broadening of the EPR resonances.[96] Using simulations, the author argued that this lack of broadening sets a maximum on the isotropic hyperfine of a coupled ^{14}N nucleus at ≈8−9 MHz, a value within our experimentally detectable range.[97]

Current proposals for native nitrogenous ligands to the OEC are limited to a Mn-coordinating imidazole nitrogen from either D1-His332 or D1-His337. It has been suggested that one or both of these residues may participate in the photoassembly of the OEC by coordinating with high-affinity, a Mn(II) ion.[92,98] In fully assembled PSII, D1-His337 has been proposed to act as the initial holding site for proton translocation, shuttling protons liberated from the OEC-substrate complex to the thylakoid lumen.[99] All mutations of D1-His332 in *Synechocystis* either greatly retard or abolish O_2-evolution activity.[89] The D1-H332E mutant is able to assemble the cluster but cannot advance past the S_2 state.[34,100] The corresponding S_2 MLS observed previously at X-band[40] and here at K_a- and Q-band is slightly narrower than that found for native or wild-type* PSII preparations (see Figure 2) due to a reduction in the effective ^{55}Mn hyperfine splitting.

This spectral change could be due to a change in the electronic ground state of the Mn(III) ion from $^5B_{1g}$ (corresponding to an empty $3d_{x^2-y^2}$ metal-centered orbital) to $^5A_{1g}$ (corresponding to an empty $3d_{z^2}$-based orbital).[27,73,101] In the mutant, it is possible that the binding of the D1-Glu332 to Mn_C changes the relative energies of the e_g orbitals leading to depopulation of the $3d_{z^2}$-based molecular orbital. Alternatively, replacing a neutral imidazole ligand with the anionic side chain of glutamate may lower the reduction potential of Mn_C relative to the other Mn-centers leading to a redistribution of oxidizing equivalents within the OEC. This intracluster electron transfer could place the formal Mn(III) ion in a sufficiently different bonding environment to yield a $^5A_{1g}$ ground state and give rise to the altered MLS. Interestingly, Cox et al. showed that the altered MLS generated by substituting Sr^{2+} for Ca^{2+} in PSII from *T. elongatus* does not result from a change in electronic ground state description of the Mn(III) ion.[30] Rather, a slight diminution of the Mn(III) ion zero-field splitting constant leads to reduction in both g-tensor and ^{55}Mn hyperfine anisotropy for the OEC. Thus, there appear to be several mechanisms that could give rise to the altered MLS.

The X-, K_a-, and Q-band ESEEM spectra of D1-H332E mutant PSII from *Synechocystis* show none of the nitrogen

isotope sensitive features observed in the spectra of wild-type* PSII (Figure 5 and Figure S1). Most simply this indicates that the source of the nitrogen coupling is from D1-His332, and upon mutation to glutamate, there is no longer a nitrogen ligand available.

Comparison of Thermophilic and Mesophilic Cyanobacterial PSII. In contrast to these findings, Boussac and coworkers recently found that mutation of D1-His332 (to either Ser or Gln) in PSII from *T. elongatus* only slightly attenuates O_2-evolution kinetics (activity is 80% of wild-type* enzyme) and does not alter the S_2 MLS.[36] Furthermore, the corresponding X-band ESEEM spectrum of *T. elongatus* D1-H332S PSII possesses what appears to be the same feature at ≈5 MHz that has been previously attributed to the OEC-coordinating histidine.[38,39] The authors thus concluded that it is D1-His337 that provides the nitrogen that is hyperfine coupled to the OEC in the S_2 state. The origin of this discrepancy between the *Synechocystis* and *T. elongatus* ESEEM results remains unclear. We do note, however, that using the ^{14}N magnetic parameters given in Table 1 to simulate an ESEEM spectrum acquired at 352 mT we expect to observe a prominent feature 4.8 MHz with a shoulder at 2.5 MHz (see Figure S4). This strongly suggests that the features previously observed at X-band excitation frequencies and those obtained by excitation at K_a- and Q-band arise from the same hyperfine-coupled nucleus.

It is unlikely that the two native enzymes have different ligand sets for the OEC. However, there is no X-ray diffraction data available for PSII isolated from *Synechocystis*. Instead, all the available crystal structures of PSII are for enzyme isolated from thermophilic cyanobacteria including *T. elongatus*. In each of the PDB files, the D1-His332 ε-N is in close proximity to Mn_C ($r_{Mn-N\varepsilon}$ = 1.99−2.49 Å) and the δ-N is H-bonded to the backbone carbonyl of D1-Glu329, locking the imidazole ring into place. Recently, the carboxylate side chain of D1-Glu329 has been postulated to take part in an extended H-bonding network involved in proton translocation.[102] Mutating D1-His332 to glutamate may perturb this network and contribute to the minor loss of O_2-evolution activity observed in *T. elongatus*.

The D1-H332E and D1-H332D mutants in *Synechocystis* are inactive, yet *Synechocystis* D1-H332S has 10−15% activity of wild-type*. The corresponding change in fluorescence and thermoluminescence properties suggests that mutating D1-His332 to a residue with a carboxylic side chain affects the communication between the electron donor side of PSII (the OEC) and the acceptor side 45 Å away, where plastoquinone is bound.[100] The serine mutant does not suffer from these effects, again pointing to the role of this side chain as a H-bond donor to the backbone of D1-Glu329 that preserves the structural relationship between the donor and acceptor sides of the charge separation pathway.

It is interesting to note that of the 112 residues within 12 Å of the $[Mn_4Ca]$ cluster[b] the only significant difference between the corresponding sequences of amino acids for the two organisms is immediately adjacent to D1-Glu329 (Table 2). In *T. elongatus* as well as *T. vulcanus* and spinach, D1−328 is a methionine whereas in *Synechocystis* this residue is a phenylalanine. Nonetheless, it is difficult to imagine how such a difference could give rise to a change in OEC ligand set.

At this time, we cannot rule out that the nitrogen responsible for the observed ESEEM is on the imidazole ring of D1-His337. Results from recent Mn-edge XAS studies that compared wild-type *Synechocystis* PSII and the D1-H332E mutants suggest that there could be significant structural perturbations—a 0.05 Å elongation of Mn···Mn internuclear distances—of the OEC upon this mutation.[103] The authors offer that such geometric changes and the corresponding changes in electronic structure (described by the altered MLS and different behaviors for electron transfer)[34,100,104] could eliminate the hyperfine coupling from D1-His337. Somehow, the PSII mutants D1-H332S and D1-H332Q from *T. elongatus* do not similarly affect the electronic structure, and the X-band nitrogen ESEEM spectrum is apparently unchanged.[36] Higher frequency studies on these *T. elongatus* mutants as well as on complementary mutants in *Synechocystis* are clearly warranted, as the results will afford a quantitative evaluation of any changes in nitrogen magnetic parameters.

Table 2. Nonidentical Amino Acid Residues within 12 Å of OEC

polypeptide →	D1					CP43		
species/residue	85	87	290	326	328	307	312	411
Synechocystis	S	N	V	I	F	P	S	I
T. elongatus	S	N	I	L	M	M	A	I
spinach	T	A	I	L	M	P	A	A

Other *T. elongatus* PSII D1 mutants seem to preserve characteristics of the wild-type enzyme whereas the corresponding mutants in *Synechocystis* exhibit dramatically different properties. One such example is D1-His198, which serves as the axial ligand to Mg in chlorophyll D1 that makes up part of P_{680}, the primary electron donor in PSII. In *Synechocystis*, the mutants D1-H198A and D1-H198Q change the absorption spectrum of P_{680} and affect its reduction potential.[105] In *T. elongatus*, these mutations have little effect.[106] The side chain of D1-Glu130 is a H-bonding partner to pheophytin bound in D1 ($Pheo_{D1}$). The D1-Q130E substitution in *T. elongatus* has no effect on the kinetics and thermodynamics of electron transfer involving $Pheo_{D1}$,[106] whereas in *Synechocystis*, this mutant changes the pheophytin reduction potential by ≈38 meV.[107,108] In these cases, it seems that mutation of ligands to redox-active cofactors leads to significant changes in the mesophilic cyanobacterium *Synechocystis*, but through some unknown mechanism, the thermophilic *T. elongatus* is largely immune.

Why Is Histidine a Ligand to the OEC? Excepting PSII, all known Mn-based oxidoreductases (e.g., Mn-superoxide dismutase,[109] Mn-ribonucleotide reductase (RNR),[110] and the dimanganese catalase[111]) employ at least one histidine residue as a ligand to each Mn ion that makes up the active site. One possible reason for this is that the neutral charge and intermediate Lewis softness of the imidazole ring (assuming the distal nitrogen retains its proton) prevents the coordinating Mn ion from being oxidized beyond the 3+ oxidation state. Anionic ligands such as carboxylates and cystienates, on the other hand, bind strongly to and help stabilize the charge of higher oxidation states of coordinating metal ions. For example, in 2-Cys/2-His liganded Rieske-type[112,113] and even 3-Cys/1-His liganded $[Fe_2S_2]$ clusters,[97] the Fe center coordinated by histidine(s) is not the site of oxidation as the more electronegative imidazole stabilizes the ferrous ion. The relatively large amount of unpaired spin in the ^{14}N 2s-orbital ($f_{2s}(^{14}N)$ = 0.87%) is a sign of the strength of interaction between the OEC and its active-site histidine. Perhaps then, PSII exploits this relationship to keep one Mn reduced (in the 3+ oxidation state), at least until the other Mn centers of the OEC are

dx.doi.org/10.1021/bi2010703 | *Biochemistry* 2011, 50, 7390−7404

oxidized. Support for this idea is gained by the hypothesis that alternative distribution schemes of the oxidizing equivalents over the four Mn ions abort the water-oxidation mechanism at the S_2 state. For example, the altered MLS generated by D1-H332E site-directed mutagenesis of *Synechocystis* PSII (Figure 2) can be rationalized in terms of a change in the location of the Mn(III) ion within the cluster.[27] This would of course change the location of the Jahn−Teller axis and possibly lead to the perturbation of Mn···Mn distances seen in the EXAFS of the D1-H332E mutant.[103]

Protic ligands such as histidine can also activate metal-bound substrates. As one example, kinetic studies of eukaryotic arginase revealed that mutations of amino acids hydrogen-bonded to one of the metal-coordinating histidines could dramatically affect the Lewis acidity of the metal ion and enhance the rate of arginine hydrolysis.[114] Deprotonation of imidazole-like ligands on a Ru(II) complex was found to destabilize occupied metal-centered π-donor orbitals allowing for stronger interaction with the formally unoccupied C−H antibonding orbital of the substrate.[115] If Mn_C also coordinated one of the substrate waters, one can imagine that the above mechanisms would (i) enhance formation of a metal-bound hydroxo species and (ii) activate the O−H bond for insertion of an oxygen atom derived from the other OEC-bound substrate moiety. This would generate a Mn-peroxo intermediate of the type that has been proposed based on results from studies that attempted to drive S_0 back to an S_4-like state using high O_2 pressure.[116,117]

CONCLUSIONS

The nitrogen isotope sensitive features found in the K_a- and Q-band ESEEM spectra of PSII from *Synechocystis* PCC 6803 are conclusively assigned to an active site histidine residue. In particular, our analysis of the effective hyperfine coupling points to the lone Mn(III) ion present in the S_2 state as being the bonding partner with histidine. Whether the observed coupling arises from an imidazole nitrogen of D1-His332 or D1-His337 cannot be determined definitively from our data. What is known is that mutation of D1-His332 in PSII from *Synechocystis* leads to significant reduction in oxygen-evolving activity and dramatic changes in electronic structure—loss of all nitrogen isotope sensitive features and possibly a redistribution of oxidizing equivalents around the OEC. For currently unknown reasons, mutations of the same residue in *T. elongatus* have only modest effect on these fronts.

The nitrogen magnetic coupling parameters reported here (see Table 1) are valuable in evaluating DFT models of the OEC in the S_2 state.[118−120] Recently, such calculations have been assessed based on agreement of computed ^{55}Mn hyperfine coupling constants with those derived from multifrequency ENDOR studies.[121,122] Ligand HFI, however, is a more discriminatory means by which to judge the computed structures. By selectively introducing magnetic nuclei in positions about the OEC[35] (or taking advantage of naturally occurring ones such as the nitrogens in histidine), we can characterize magnetic interactions that will be extremely sensitive to the spin topology of the cluster. Interestingly, an energetically competent computational model of the OEC developed by Siegbahn shows that Mn_C can be a substrate binding site, is the location of the Mn(III) ion in the S_2 state, and is coordinated D1-His332.[119] This model is consistent with many spectroscopic results including those from EXAFS and ^{55}Mn ENDOR studies.[29,30] Importantly, the Siegbahn model also comes closest to predicting the strength of the ^{14}N hyperfine and nuclear quadrupole interactions reported here.[120]

Note Added during Review. While this manuscript was under review, the 1.9 Å resolution crystal structure of PSII from *T. vulcanus* was deposited in the Protein Data Bank (accession code 3ARC) and discussed in a corresponding paper.[16] These data were collected under conditions in which reduction of the cluster due to the incident X-ray beam is greatly diminished compared to earlier crystallography studies. This technique afforded unparalleled resolution of the electron density of the OEC including the identification of five oxo bridges. However, the reported dosing rate still suggests that some Mn-centered reduction occurs (personal communication with Junko Yano and Johannes Messinger).[14] As with all preceding crystal structures, the imidazole side chain of D1-His332 is shown to be bound directly to one of the Mn centers of the cluster (Mn_C, Figure 6). The ε-nitrogen of D1-His337, on the other hand, appears to be H-bonded to the μ_3-oxo group that bridges the three Mn ions found within the cuboidal part of the OEC. Perpendicular to the Mn_C-N_{His332} bonding vector is a very long Mn_C−oxo bond of 2.60 Å, leading to an almost square-pyramidal ligand field for Mn_C. As described in the Discussion section, the strength of the ^{14}N hyperfine interaction reported here and previously[41,42] is consistent with the histidine being an equatorial ligand to either a square-pyramidal or tetragonally elongated pseudo-octahedral Mn(III) ion (i.e., with a $^5B_{1g}$ ground state).

ASSOCIATED CONTENT

Supporting Information

Additional K_a-band ESEEM spectra collected at other field positions; Q-band ESE EPR and ESEEM spectra along with corresponding simulations; simulations of cyt b_{559} contributions to ESEEM data. This material is available free of charge via the Internet at http://pubs.acs.org.

AUTHOR INFORMATION

Corresponding Author

*Phone: 530-752-6377. Fax: 530-752-8995. E-mail: rdbritt@ucdavis.edu.

Author Contributions

⊥These authors contributed equally to this work.

Funding

This work was funded by the National Institutes of Health grant GM-048242 to R.D.B. and grant GM-076232 to R.J.D. and the Division of Chemical Sciences, Geosciences, and Biosciences, Office of Basic Energy Sciences, U.S. Department of Energy, grant DE-FG02-10ER16191 to R.J.D. The EPR spectrometers used in this study are part of the CalEPR center and were funded by NIH grants GM-061211 and S10-RR021075 and the University of California at Davis.

ACKNOWLEDGMENTS

We are grateful to Anh P. Nguyen for preparing the thylakoid membranes from *Synechocystis* used by R.J.S. and to Robert M. McCarrick for preparing the thylakoid membranes from spinach used by G.J.Y.

ABBREVIATIONS

EPR, electron paramagnetic resonance; ENDOR, electron nuclear double resonance; ESEEM, electron spin-echo

envelope modulation; EXAFS, extended X-ray absorption fine structure; FTIR, Fourier transform infrared spectroscopy; HFI, hyperfine interaction; MLS, multiline signal; NQI, nuclear quadrupole interaction; PSII, photosystem II; OEC, oxygen-evolving complex; XAS, X-ray absorption spectroscopy.

■ ADDITIONAL NOTES

[†]Some of these results were presented earlier in a conference proceedings report that was not peer-reviewed.

[a]The initial report was presented at the 15th International Congress of Photosynthesis in Beijing, China, by J.-R. Shen, Y. Umena, K. Kawakami, and N. Kamiya (poster PS6.5).

[b]Specifically, this sphere includes D1-58−67, 83−90, 112, 157−173, 178−191, 290−297, 325−344; D2-312−321, 349−352; and CP43-306−313, 352−358, 399−401, 410−412 (using 3KZI). Overall, there are 21 differences in the D1 sequence between *Synechocystis* sp. PCC 6803 and *T. elongatus*.

[c]Wild-type* refers to PSII isolated from a control strain of *Synechocystis* sp. PCC 6803 constructed in identical fashion as the D1-H332E mutant, but containing the wild-type psbA-2 gene.

■ REFERENCES

(1) Yeagle, G. J., Gilchrist, M. L. Jr., Walker, L. M., Debus, R. J., and Britt, R. D. (2008) Multifrequency electron spin-echo envelope modulation studies of nitrogen ligation to the manganese cluster of photosystem II. *Philos. Trans. R. Soc., B 363*, 1157−1166.

(2) Diner, B. A. (2001) Amino acid residues involved in the coordination and assembly of the manganese cluster of photosystem II. Proton-coupled electron transport of the redox-active tyrosines and its relationship to water oxidation. *Biochim. Biophys. Acta, Bioenerget. 1503*, 147−163.

(3) Debus, R. J. (2001) Amino acid residues that modulate the properties of tyrosine Y_Z and the manganese cluster in the water oxidizing complex of photosystem II. *Biochim. Biophys. Acta, Bioenerget. 1503*, 164−186.

(4) Debus, R. J. (2008) Protein ligation of the photosynthetic oxygen-evolving center. *Coord. Chem. Rev. 252*, 244−258.

(5) Zouni, A., Witt, H.-T., Kern, J., Fromme, P., Krauss, N., Saenger, W., and Orth, P. (2001) Crystal structure of photosystem II from *Synechococcus elongatus* at 3.8 Å resolution. *Nature 409*, 739−743.

(6) Kamiya, N., and Shen, J.-R. (2003) Crystal structure of oxygen-evolving photosystem II from *Thermosynechococcus vulcanus* at 3.7 Å resolution. *Proc. Natl. Acad. Sci. U. S. A. 100*, 98−103.

(7) Ferreira, K. N., Iverson, T. M., Maghlaoui, K., Barber, J., and Iwata, S. (2004) Architecture of the photosynthetic oxygen-evolving center. *Science 303*, 1831−1838.

(8) Loll, B., Kern, J., Saenger, W., Zouni, A., and Biesiadka, J. (2005) Towards complete cofactor arrangement in the 3.0 Å resolution structure of photosystem II. *Nature 438*, 1040−1044.

(9) Kern, J., Loll, B., Zouni, A., Saenger, W., Irrgang, K.-D., and Biesiadka, J. (2005) Cyanobacterial photosystem II at 3.2 Å resolution - the plastoquinone binding pockets. *Photosynth. Res. 84*, 153−159.

(10) Kawakami, K., Umena, Y., Kamiya, N., and Shen, J. R. (2009) Location of chloride and its possible functions in oxygen-evolving photosystem II revealed by X-ray crystallography. *Proc. Natl. Acad. Sci. U. S. A. 106*, 8567−8572.

(11) Guskov, A., Kern, J., Gabdulkhakov, A., Broser, M., Zouni, A., and Saenger, W. (2009) Cyanobacterial photosystem II at 2.9 Å resolution and the role of quinones, lipids, channels and chloride. *Nat. Struct. Mol. Biol. 16*, 334−342.

(12) Murray, J. W., Maghlaoui, K., Kargul, J., Ishida, N., Lai, T. L., Rutherford, A. W., Sugiura, M., Boussac, A., and Barber, J. (2008) X-ray crystallography identifies two chloride binding sites in the oxygen-evolving centre of photosystem II, *Energ. Environ. Sci. 1*, 161−166.

(13) Guskov, A., Broser, M., Gabdulkhakov, A., Kern, J., Zouni, A., Loll, B., Biesiadka, J., and Saenger, W. (2007) X-ray crystallographic analysis of PSII from *T. elongatus* at 3.0 Å resolution. *Photosynth. Res. 91*, PS422.

(14) Yano, J., Kern, J., Irrgang, K.-D., Latimer, M. J., Bergmann, U., Glatzel, P., Pushkar, Y., Biesiadka, J., Loll, B., Sauer, K., Messinger, J., Zouni, A., and Yachandra, V. K. (2005) X-ray damage to the Mn_4Ca complex in single crystals of photosystem II: A case study for metalloprotein crystallography. *Proc. Natl. Acad. Sci. U. S. A. 102*, 12047−12052.

(15) Grabolle, M., Haumann, M., Müller, C., Liebisch, P., and Dau, H. (2006) Rapid loss of structural motifs in the manganese complex of oxygenic photosynthesis by X-ray irradiation at 10−300 K. *J. Biol. Chem. 281*, 4580−4588.

(16) Umena, Y., Kawakami, K., Shen, J.-R., and Kamiya, N. (2011) Crystal structure of oxygen-evolving photosystem II at a resolution of 1.9 Å. *Nature 473*, 55−60.

(17) Dismukes, G. C., and Siderer, Y. (1980) EPR spectroscopic observations of a manganese center associated with water oxidation in spinach chloroplasts. *FEBS Lett. 121*, 78−80.

(18) Dismukes, G. C., and Siderer, Y. (1981) Intermediates of a polynuclear manganese center involved in photosynthetic oxidation of water. *Proc. Natl. Acad. Sci. U. S. A. 78*, 274−278.

(19) Dismukes, G. C., Ferris, K., and Watnick, P. (1982) EPR spectroscopic evidence for a tetranuclear manganese cluster as the site for photosynthetic oxygen evolution. *Photobiochem. Photobiophys. 3*, 243−256.

(20) Rutherford, A. W., Boussac, A., and Zimmermann, J. L. (1991) EPR studies of the oxygen evolving enzyme. *New J. Chem. 15*, 491−500.

(21) Miller, A. F., and Brudvig, G. W. (1991) A guide to electron paramagnetic resonance spectroscopy of photosystem II membranes. *Biochim. Biophys. Acta, Bioenerget. 1056*, 1−18.

(22) Britt, R. D., Peloquin, J. M., and Campbell, K. A. (2000) Pulsed and parallel-polarization EPR characterization of the photosystem II oxygen-evolving complex. *Annu. Rev. Biophys. Biomol. Struct. 29*, 463−495.

(23) Peloquin, J. M., and Britt, R. D. (2001) EPR/ENDOR characterization of the physical and electronic structure of the OEC Mn cluster. *Biochim. Biophys. Acta 1503*, 96−111.

(24) Kawamori, A. (2003) Electron transfer and structure of plant photosystem II, *Prog. Theor. Chem. Phys. 10*, 529−563.

(25) Britt, R. D., Campbell, K. A., Peloquin, J. M., Gilchrist, M. L., Aznar, C. P., Dicus, M. M., Robblee, J., and Messinger, J. (2004) Recent pulsed EPR studies of the Photosystem II oxygen-evolving complex: implications as to water oxidation mechanisms. *Biochim. Biophys. Acta 1655*, 158−171.

(26) Haddy, A. (2007) EPR spectroscopy of the manganese cluster of photosystem II. *Photosynth. Res. 92*, 357−368.

(27) Peloquin, J. M., Campbell, K. A., Randall, D. W., Evanchik, M. A., Pecoraro, V. L., Armstrong, W. H., and Britt, R. D. (2000) ^{55}Mn ENDOR of the S_2-state multiline EPR signal of photosystem II: Implications on the structure of the tetranuclear Mn cluster. *J. Am. Chem. Soc. 122*, 10926−10942.

(28) Kulik, L. V., Epel, B., Lubitz, W., and Messinger, J. (2005) ^{55}Mn pulse ENDOR at 34 GHz of the S_0 and S_2 states of the oxygen-evolving complex in photosystem II. *J. Am. Chem. Soc. 127*, 2392−2393.

(29) Su, J. H., Cox, N., Ames, W., Pantazis, D. A., Rapatskiy, L., Lohmiller, T., Kulik, L. V., Dorlet, P., Rutherford, A. W., Neese, F., Boussac, A., Lubitz, W., and Messinger, J. (2011) The electronic structures of the S_2 states of the oxygen-evolving complexes of

photosystem II in plants and cyanobacteria in the presence and absence of methanol. *Biochim. Biophys. Acta, Bioenerget. 107*, 829−840.

(30) Cox, N., Rapatskiy, L., Su, J. H., Pantazis, D. A., Sugiura, M., Kulik, L., Dorlet, P., Rutherford, A. W., Neese, F., Boussac, A., Lubitz, W., and Messinger, J. (2011) Effect of Ca^{2+}/Sr^{2+} substitution on the electronic structure of the oxygen-evolving complex of photosystem II: A combined multifrequency EPR, ^{55}Mn-ENDOR, and DFT Study of the S_2 State. *J. Am. Chem. Soc. 133*, 3635−3648.

(31) Haddy, A., Lakshmi, K. V., Brudvig, G. W., and Frank, H. A. (2004) Q-band EPR of the S_2 state of photosystem II confirms an $S = 5/2$ origin of the X-band $g = 4.1$ signal. *Biophys. J. 87*, 2885−2896.

(32) Beck, W. F., and Brudvig, G. W. (1986) Binding of amines to the oxygen-evolving center of photosystem II. *Biochemistry 25*, 6479−6486.

(33) Cole, J., Yachandra, V. K., Guiles, R. D., McDermott, A. E., Britt, R. D., Dexheimer, S. L., Sauer, K., and Klein, M. P. (1987) Assignment of the $g = 4.1$ EPR signal to manganese in the S_2 state of the photosynthetic oxygen-evolving complex: An x-ray absorption edge spectroscopy study. *Biochim. Biophys. Acta, Bioenerget. 890*, 395−398.

(34) Debus, R. J., Campbell, K. A., Peloquin, J. M., Pham, D. P., and Britt, R. D. (2000) Histidine 332 of the D1 polypeptide modulates the magnetic and redox properties of the manganese cluster and tyrosine Y_Z in photosystem II. *Biochemistry 39*, 470−478.

(35) Stull, J. A., Stich, T. A., Service, R. J., Debus, R. J., Mandal, S. K., Armstrong, W. H., and Britt, R. D. (2010) ^{13}C ENDOR reveals that the D1 polypeptide C-terminus is directly bound to Mn in the photosystem II oxygen evolving complex. *J. Am. Chem. Soc. 132*, 446−447.

(36) Sugiura, M., Rappaport, F., Hillier, W., Dorlet, P., Ohno, Y., Hayashi, H., and Boussac, A. (2009) Evidence that D1-His332 in photosystem II from *Thermosynechococcus elongatus* interacts with the S_3 state and not with the S_2 state. *Biochemistry 48*, 7856−7866.

(37) Service, R. J., Yano, J., McConnell, I., Hwang, H. J., Niks, D., Hille, R., Wydrzynski, T., Burnap, R. L., Hillier, W., and Debus, R. J. (2011) Participation of glutamate-354 of the CP43 polypeptide in the ligation of manganese and the binding of substrate water in photosystem II. *Biochemistry 50*, 63−81.

(38) DeRose, V. J., Yachandra, V. K., McDermott, A. E., Britt, R. D., Sauer, K., and Klein, M. P. (1991) Nitrogen ligation to manganese in the photosynthetic oxygen-evolving complex: Continuous-wave and pulsed EPR studies of photosystem II particles containing nitrogen-14 or nitrogen-15. *Biochemistry 30*, 1335−1341.

(39) Tang, X. S., Diner, B. A., Larsen, B. S., Gilchrist, M. L. Jr., Lorigan, G. A., and Britt, R. D. (1994) Identification of histidine at the catalytic site of the photosynthetic oxygen-evolving complex. *Proc. Natl. Acad. Sci. U. S. A. 91*, 704−708.

(40) Debus, R. J., Campbell, K. A., Gregor, W., Li, Z.-L., Burnap, R. L., and Britt, R. D. (2001) Does histidine 332 of the D1 polypeptide ligate the manganese cluster in photosystem II? An electron spin echo envelope modulation study. *Biochemistry 40*, 3690−3699.

(41) Yeagle, G. J., Gilchrist, M. L., McCarrick, R. M., and Britt, R. D. (2008) Multifrequency pulsed electron paramagnetic resonance study of the S_2 state of the photosystem II manganese cluster. *Inorg. Chem. 47*, 1803−1814.

(42) Milikisiyants, S., Chatterjee, R., Weyers, A., Meenaghan, A., Coates, C., and Lakshmi, K. V. (2010) Ligand environment of the S_2 state of photosystem II: A study of the hyperfine interactions of the tetranuclear manganese cluster by 2D ^{14}N HYSCORE spectroscopy. *J. Phys. Chem. B 114*, 10905−10911.

(43) Åhrling, K. A., Evans, M. C. W., Nugent, J. H. A., Ball, R. J., and Pace, R. J. (2006) ESEEM studies of substrate water and small alcohol binding to the oxygen-evolving complex of photosystem II during functional turnover. *Biochemistry 45*, 7069−7082.

(44) Flanagan, H. L., Gerfen, G. J., and Singel, D. J. (1988) Multifrequency electron spin-echo envelope modulation: The determination of nitro group nitrogen-14 hyperfine and quadrupole interactions of DPPH in frozen solution. *J. Chem. Phys. 88*, 20−24.

(45) Chu, H.-A., Debus, R. J., and Babcock, G. T. (2001) D1-Asp170 is structurally coupled to the oxygen evolving complex in photosystem II as revealed by light-induced Fourier transform infrared difference spectroscopy. *Biochemistry 40*, 2312−2316.

(46) Rippka, R., Deruelles, J., Waterbury, J. B., Herdman, M., and Stanier, R. Y. (1979) Generic assignments, strain histories, and properties of pure cultures of cyanobacteria. *J. Gen. Microbiol. 111*, 1−61.

(47) Strickler, M. A., Walker, L. M., Hillier, W., Britt, R. D., and Debus, R. J. (2007) No evidence from FTIR difference spectroscopy that aspartate-342 of the D1 polypeptide ligates a Mn ion that undergoes oxidation during the S_0 to S_1, S_1 to S_2, or S_2 to S_3 transitions in photosystem II. *Biochemistry 46*, 3151−3160.

(48) Yamanari, T., Kimura, Y., Mizusawa, N., Ishii, A., and Ono, T. (2004) Mid- to low-frequency Fourier transform infrared spectra of S-state cycle for photosynthetic water oxidation in *Synechocystis* sp. PCC 6803. *Biochemistry 43*, 7479−7490.

(49) Strickler, M. A., Walker, L. M., Hillier, W., and Debus, R. J. (2005) Evidence from biosynthetically incorporated strontium and FTIR difference spectroscopy that the C-terminus of the D1 polypeptide of photosystem II does not ligate calcium. *Biochemistry 44*, 8571−8577.

(50) Chu, H.-A., Nguyen, A. P., and Debus, R. J. (1994) Site-directed photosystem II mutants with perturbed oxygen-evolving properties. 1. Instability or inefficient assembly of the manganese cluster *in vivo*. *Biochemistry 33*, 6137−6149.

(51) Berthold, D. A., Babcock, G. T., and Yocum, C. F. (1981) A highly resolved, oxygen-evolving photosystem II preparation from spinach thylakoid membranes. EPR and electron-transport properties. *FEBS Lett. 134*, 231−234.

(52) Ford, R. C., and Evans, M. C. W. (1983) Isolation of a photosystem 2 preparation from higher plants with highly enriched oxygen evolution activity. *FEBS Lett. 160*, 159−164.

(53) Campbell, K. A., Gregor, W., Pham, D. P., Peloquin, J. M., Debus, R. J., and Britt, R. D. (1998) The 23 and 17 kDa Extrinsic Proteins of Photosystem II Modulate the Magnetic Properties of the S1-State Manganese Cluster. *Biochemistry 37*, 5039−5045.

(54) Dasneves, H. J. C., and Vasconcelos, A. M. P. (1987) Capillary gas chromotography of amino acids, including asparagine and glutamine - Sensitive gas chromatographic mass spectrometric and selected ion monitoring gas chromatographic mass spectrometric detection of the N,O(S)-tert(S)-tert-butyldimethylsilyl derivatives. *J. Chromatogr. 392*, 249−258.

(55) Stich, T. A., Lahiri, S., Yeagle, G., Dicus, M., Brynda, M., Gunn, A., Aznar, C., DeRose, V. J., and Britt, R. D. (2007) Multifrequency pulsed EPR studies of biologically relevant manganese(II) complexes. *Appl. Magn. Reson. 31*, 321−341.

(56) Peloquin, J. M., Tang, X. S., Diner, B. A., and Britt, R. D. (1999) An Electron Spin-Echo Envelope Modulation (ESEEM) Study of the QA Binding Pocket of PS II Reaction Centers from Spinach and Synechocystis. *Biochemistry 38*, 2057−2067.

(57) Mims, W. B. (1984) Elimination of the dead-time artifact in electron spin-echo envelope spectra. *J. Magn. Reson. 59*, 291−306.

(58) Stoll, S., and Schweiger, A. (2006) EasySpin, a comprehensive software package for spectral simulation and analysis in EPR. *J. Magn. Reson. 178*, 42−55.

(59) Stoll, S., and Britt, R. D. (2009) General and efficient simulation of pulse EPR spectra. *Phys. Chem. Chem. Phys. 11*, 6614−6625.

(60) García-Rubio, I., Martínez, J. I., Picorel, R., Yruela, I. L., and Alonso, P. J. (2003) HYSCORE spectroscopy in the cytochrome b_{559} of the photosystem II reaction center. *J. Am. Chem. Soc. 125*, 15846−15854.

(61) Smith, P. J., Åhrling, K. A., and Pace, R. J. (1993) Nature of the S_2 state electron paramagnetic resonance signals from the oxygen-evolving

complex of photosystem II: Q-band and oriented X-band studies. *J. Chem. Soc., Faraday Trans. 89*, 2863−2868.

(62) Teutloff, C., Kessen, S., Kern, J., Zouni, A., and Bittl, R. (2006) High-field (94-GHz) EPR spectroscopy on the S_2 multiline signal of photosystem II. *FEBS Lett. 580*, 3605−3609.

(63) Matsuoka, H., Furukawa, K., Kato, T., Mino, H., Shen, J.-R., and Kawamori, A. (2006) *g*-Anisotropy of the S_2-state manganese cluster in single crystals of cyanobacterial photosystem II studied by W-band electron paramagnetic resonance spectroscopy. *J. Phys. Chem. B 110*, 13242−13247.

(64) Lai, A., Flanagan, H. L., and Singel, D. J. (1988) Multifrequency electron spin echo envelope modulation is $S = 1/2$, $I = 1/2$ systems - Analysis of the spectral amplitudes, line-shapes, and linewidths. *J. Chem. Phys. 89*, 7161−7166.

(65) Scholes, C. P., Lapidot, A., Mascarenhas, R., Inubushi, T., Isaacson, R. A., and Feher, G. (1982) Electron nulcear double resonance (ENDOR) from heme and histidine nitrogens in single crystals of aquometmyoglobin. *J. Am. Chem. Soc. 104*, 2724−2735.

(66) Chu, H.-A., Hillier, W., and Debus, R. J. (2004) Evidence that the C-terminus of the D1 polypeptide of photosystem II is ligated to the manganese ion that undergoes oxidation during the S_1 to S_2 transition: An isotope-edited FTIR study. *Biochemistry 43*, 3152−3166.

(67) Campbell, K. A., Peloquin, J. M., Diner, B. A., Tang, X.-S., Chisholm, D. A., and Britt, R. D. (1997) The τ-nitrogen of D2 histidine 189 is the hydrogen bond donor to the tyrosine radical $Y_D^{\cdot}$ of photosystem II. *J. Am. Chem. Soc. 119*, 4787−4788.

(68) Beck, W. F., De Paula, J. C., and Brudvig, G. W. (1986) Ammonia binds to the manganese site of the oxygen-evolving complex of photosystem II in the S_2 state. *J. Am. Chem. Soc. 108*, 4018−4022.

(69) Boussac, A., and Rutherford, A. W. (1988) Nature of the inhibition of the oxygen-evolving enzyme of photosystem II induced by sodium chloride washing and reversed by the addition of calcium(2+) or strontium(2+). *Biochemistry 27*, 3476−3483.

(70) Debus, R. J., Aznar, C., Campbell, K. A., Gregor, W., Diner, B. A., and Britt, R. D. (2003) Does aspartate 170 of the D1 polypeptide ligate the manganese cluster in photosystem II? An EPR and ESEEM study. *Biochemistry 42*, 10600−10608.

(71) Boerner, R. J., Nguyen, A. P., Barry, B. A., and Debus, R. J. (1992) Evidence from directed mutagenesis that aspartate 170 of the D1 polypeptide influences the assembly and/or stability of the manganese cluster in the photosynthetic water-splitting complex. *Biochemistry 31*, 6660−6672.

(72) Nixon, P. J., and Diner, B. A. (1992) Aspartate 170 of the photosystem II reaction center polypeptide D1 is involved in the assembly of the oxygen-evolving manganese cluster. *Biochemistry 31*, 942−948.

(73) Campbell, K. A., Force, D. A., Nixon, P. J., Dole, F., Diner, B. A., and Britt, R. D. (2000) Dual-mode EPR detects the initial intermediate in photoassembly of the photosystem II Mn cluster: The influence of amino acid residue 170 of the D1 polypeptide on Mn coordination. *J. Am. Chem. Soc. 122*, 3754−3761.

(74) Hwang, H. J., McLain, A., Debus, R. J., and Bumap, R. L. (2007) Photoassembly of the manganese cluster in mutants perturbed in the high affinity Mn-binding site of the H_2O-oxidation complex of photosystem II. *Biochemistry 46*, 13648−13657.

(75) Stich, T. A., Whittaker, J. W., and Britt, R. D. (2010) Multifrequency EPR studies of manganese catalases provide a complete description of proteinaceous nitrogen coordination. *J. Phys. Chem. B 114*, 14178−14188.

(76) Tan, X. L., Gultneh, Y., Sarneski, J. E., and Scholes, C. P. (1991) EPR-ENDOR of the electronic structure from 2 nitrogenously ligated bis(μ-oxo)$Mn^{III}Mn^{IV}$ model complexes spectroscopically relevant to the multi-manganese center of photosytem II. *J. Am. Chem. Soc. 113*, 7853−7858.

(77) Sinnecker, S., Neese, F., and Lubitz, W. (2005) Dimanganese catalase-spectroscopic parameters from broken-symmetry density functional theory of the superoxidized MnIII/MnIV state. *J. Biol. Inorg. Chem. 10*, 231−238.

(78) Sinnecker, S., Neese, F., Noodleman, L., and Lubitz, W. (2004) Calculating the electron paramagnetic resonance parameters of exchange coupled transition metal complexes using broken symmetry density functional theory: Application to a MnIII/MnIV model compound. *J. Am. Chem. Soc. 126*, 2613−2622.

(79) Randall, D. W. (1998) Pulsed EPR Studies of Tyrosine Radicals and Manganese Complexes: Insights into Photosynthetic Oxygen Evolution, University of California—Davis, Davis, CA.

(80) Bencini, A., and Gatteschi, D. (1990) *EPR of Exchange Coupled Systems*, Springer, Berlin.

(81) Orio, M., Pantazis, D. A., Petrenko, T., and Neese, F. (2009) Magnetic and spectroscopic properties of mixed valence manganese-(III,IV) dimers: A systematic study using broken symmetry density functional theory. *Inorg. Chem. 48*, 7251−7260.

(82) Morton, J. R., and Preston, K. F. (1978) Atomic paramaters for paramagnetic resonance data. *J. Magn. Reson. 30*, 577−582.

(83) Lorigan, G. A., and Britt, R. D. (1994) Temperature-dependent pulsed electron paramagnetic resonance studies of the S_2 state multiline signal of the photosynthetic oxygen-evolving complex. *Biochemistry 33*, 12072−12076.

(84) Ashby, C. I. H., Cheng, C. P., and Brown, T. L. (1978) Nitrogen-14 nuclear quadrupole resonance spectra of coordinated imidazole. *J. Am. Chem. Soc. 100*, 6057−6063.

(85) Aasa, R., Andreasson, L. E., Lagenfelt, G., and Vanngard, T. (1987) A comparison between the multiline EPR signals of spinach and *Anacystis nidulans* and their temperature dependence. *FEBS Lett. 221*, 245−248.

(86) Yano, J., and Yachandra, V. (2007) Oxidation state changes of the Mn_4Ca cluster in photosystem II. *Photosynth. Res. 92*, 289−303.

(87) Pushkar, Y. L., Yano, J., Sauer, K., Boussac, A., and Yachandra, V. K. (2008) Structural changes in the Mn_4Ca cluster and the mechanism of photosynthetic water splitting. *Proc. Natl. Acad. Sci. U. S. A. 105*, 1879−1884.

(88) Mizusawa, N., Yamanari, T., Kimura, Y., Ishii, A., Nakazawa, S., and Ono, T.-A. (2004) Changes in the functional and structural properties of the Mn cluster induced by replacing the side group of the C-terminus of the D1 protein of photosystem II. *Biochemistry 43*, 14644−14652.

(89) Chu, H.-A., Nguyen, A. P., and Debus, R. J. (1994) Site-directed photosystem II mutants with perturbed oxygen-evolving properties. 2. Increased binding or photooxidation of manganese in the absence of the extrinsic 33-kDa polypeptide *in vivo*. *Biochemistry 33*, 6150−6157.

(90) Chu, H.-A., Nguyen, A. P., and Debus, R. J. (1995) Amino acid residues that influence the binding of manganese or calcium to photosystem II. 1. The lumenal interhelical domains of the D1 polypeptide. *Biochemistry 34*, 5839−5858.

(91) Diner, B. A., and Nixon, P. J. (1992) The rate of reduction of oxidized redox-active tyrosine, Z+, by exogenous manganese(2+) is slowed in a site-directed mutant, at aspartate 170 of polypeptide D1 of photosystem II, inactive for photosynthetic oxygen evolution. *Biochim. Biophys. Acta, Bioenerget. 1101*, 134−138.

(92) Ghirardi, M. L., Lutton, T. W., and Seibert, M. (1998) Effects of carboxyl amino acid modification on the properties of the high-affinity, manganese-binding site in photosystem II. *Biochemistry 37*, 13559−13566.

(93) Debus, R. J., Strickler, M. A., Walker, L. M., and Hillier, W. (2005) No evidence from FTIR difference spectroscopy that aspartate-170 of the D1 polypeptide ligates a manganese ion that undergoes oxidation during the S_0 to S_1, S_1 to S_2, or S_2 to S_3 transitions in photosystem II. *Biochemistry 44*, 1367−1374.

(94) Sproviero, E. M., Gascon, J. A., McEvoy, J. P., Brudvig, G. W., and Batista, V. S. (2008) Computational studies of the O_2-evolving complex of photosystem II and biomimetic oxomanganese complexes. *Coord. Chem. Rev. 252*, 395−415.

(95) Stoll, S., Calle, C., Mitrikas, G., and Schweiger, A. (2005) Peak suppression in ESEEM spectra of multinuclear spin systems. *J. Magn. Reson. 177*, 93−101.

(96) Andreasson, L. E. (1989) Is nitrogen liganded to manganese in the photosynthetic oxygen-evolving system? EPR studies after isotopic replacement with nitrogen-15. *Biochim. Biophys. Acta, Bioenerget. 973*, 465−467.

(97) Dicus, M. M., Conlan, A., Nechushtai, R., Jennings, P. A., Paddock, M. L., Britt, R. D., and Stoll, S. (2010) Binding of histidine in the Cys_3His_1-coordinated 2Fe-2S cluster of human mitoNEET. *J. Am. Chem. Soc. 132*, 2037−2049.

(98) Cohen, R. O., Nixon, P. J., and Diner, B. A. (2007) Participation of the C-terminal region of the D1-polypeptide in the first steps in the assembly of the Mn_4Ca cluster of photosystem II. *J. Biol. Chem. 282*, 7209−7218.

(99) Kusunoki, M. (2007) Mono-manganese mechanism of the photosystem II water splitting reaction by a unique Mn_4Ca cluster. *Biochim. Biophys. Acta, Bioenerget. 1767*, 484−492.

(100) Allahverdiyeva, Y., Deak, Z., Szilard, A., Diner, B. A., Nixon, P. J., and Vass, I. (2004) The function of D1-H332 in photosystem II electron transport studied by thermoluminescence and chlorophyll fluorescence in site-directed mutants of *Synechocystis* 6803. *Eur. J. Biochem. 271*, 3523−3532.

(101) Campbell, K. A., Lashley, M. R., Wyatt, J. K., Nantz, M. H., and Britt, R. D. (2001) Dual-mode EPR study of Mn(III) salen and the Mn(III) salen-catalyzed epoxidation of cis-beta-methylstyrene. *J. Am. Chem. Soc. 123*, 5710−5719.

(102) Service, R. J., Hillier, W., and Debus, R. J. (2010) Evidence from FTIR difference spectroscopy of an extensive network of hydrogen bonds near the oxygen-evolving Mn_4Ca cluster of photosystem II Involving D1-Glu65, D2-Glu312, and D1-Glu329. *Biochemistry 49*, 6655−6669.

(103) Yano, J., Walker, L. M., Strickler, M. A., Service, R. J., Yachandra, V. K., and Debus, R. J. (2011) Altered structure of the Mn_4Ca cluster in the oxygen-evolving complex of photosystem II by a histidine ligand mutation. *J. Biol. Chem. 286*, 9257−9267.

(104) Chu, H.-A., Nguyen, A. P., and Debus, R. J. (1995) Amino acid residues that influence the binding of manganese or calcium to photosystem II. 2. The carboxy-terminal domain of the D1 polypeptide. *Biochemistry 34*, 5859−5882.

(105) Diner, B. A., Schlodder, E., Nixon, P. J., Coleman, W. J., Rappaport, F., Lavergne, J., Vermaas, W. F., and Chisholm, D. A. (2001) Site-directed mutations at D1-His198 and D2-His197 of photosystem II in *Synechocystis* PCC 6803: sites of primary charge separation and cation and triplet stabilization. *Biochemistry 40*, 9265−9281.

(106) Sugiura, M., Boussac, A., Noguchi, T., and Rappaport, F. (2008) Influence of histidine-198 of the D1 subunit on the properties of the primary electron donor, P_{680}, of photosystem II in *Thermosynechococcus elongatus*. *Biochim. Biophys. Acta, Bioenerget. 1777*, 331−342.

(107) Merry, S.A. P., Nixon, P. J., Barter, L. M. C., Schilstra, M., Porter, G., Barber, J., Durrant, J. R., and Klug, D. R. (1998) Modulation of quantum yield of primary radical pair formation in photosystem II by site-directed mutagenesis affecting radical cations and anions. *Biochemistry 37*, 17439−17447.

(108) Cser, K., and Vass, I. (2007) Radiative and non-radiative charge recombination pathways in photosystem II studied by thermoluminescence and chlorophyll fluorescence in the cyanobacterium *Synechocystis* 6803. *Biochim. Biophys. Acta, Bioenerget. 1767*, 233−243.

(109) Edwards, R. A., Baker, H. M., Whittaker, M. M., Whittaker, J. W., Jameson, G. B., and Baker, E. N. (1998) Crystal structure of *Escherichia coli* manganese superoxide dismutase at 2.1 Å resolution. *J. Biol. Inorg. Chem. 3*, 161−171.

(110) Boal, A. K., Cotruvo, J. A., Stubbe, J., and Rosenzweig, A. C. (2010) Structural basis for activation of class Ib ribonucleotide reductase. *Science 329*, 1526−1530.

(111) Antonyuk, S. V., Melik-Adamyan, V. R., Popov, A. N., Lamzin, V. S., Hempstead, P. D., Harrison, R. M., Artymyuk, P. D., and Barynin, V. V. (2000) Three-dimensional structure of dimanganese catalase from *Thermus thermophilus* at 1 Å resolution. *Kristallografiya 45*, 111−122.

(112) Fee, J. A., Findling, K. L., Yoshida, T., Hille, R., Tarr, G. E., Hearshen, D. O., Dunham, W. R., Day, E. P., Kent, T. A., and Munck, E. (1984) Purification and characterization of the Rieske iron-sulfur protein from *Thermus thermophilus* - Evidence for a 2Fe-2S cluster having non-cysteine ligands. *J. Biol. Chem. 259*, 124−133.

(113) Gurbiel, R. J., Batie, C. J., Sivaraja, M., True, A. E., Fee, J. A., Hoffman, B. M., and Ballou, D. P. (1989) Electron nuclear double resonance spectroscopy of ^{15}N-enriched phthalate dioxygenase from *Pseudomonas cepacia* proves that 2 histidines are coordinated to the [2Fe-2S] Rieske-type clusters. *Biochemistry 28*, 4861−4871.

(114) Stone, E. M., Chantranupong, L., and Georgiou, G. (2010) The second-shell metal ligands of human arginase affect coordination of the nucleophile and substrate. *Biochemistry 49*, 10582−10588.

(115) Hashiguchi, B. G., Young, K. J. H., Yousufuddin, M., Goddard, W. A., and Periana, R. A. (2010) Acceleration of nucleophilic CH activation by strongly basic solvents. *J. Am. Chem. Soc. 132*, 12542−12545.

(116) Clausen, J., and Junge, W. (2004) Detection of an intermediate of photosynthetic water oxidation. *Nature 430*, 480−483.

(117) Clausen, J., Junge, W., Dau, H., and Haumann, M. (2005) Photosynthetic water oxidation at high O_2 backpressure monitored by delayed chlorophyll fluorescence. *Biochemistry 44*, 12775−12779.

(118) Schinzel, S., and Kaupp, M. (2009) Validation of broken-symmetry density functional methods for the calculation of electron paramagnetic resonance parameters of dinuclear mixed-valence $Mn^{III}Mn^{IV}$ complexes. *Can. J. Chem. 87*, 1521−1539.

(119) Siegbahn, P. E. M. (2009) Structures and energetics for O_2 formation in photosystem II. *Acc. Chem. Res. 42*, 1871−1880.

(120) Schinzel, S., Schraut, J., Arbuznikov, A. V., Siegbahn, P. E. M., and Kaupp, M. (2010) Density functional calculations of ^{55}Mn, ^{14}N and ^{13}C electron paramagnetic resonance parameters support an energetically feasible model system for the S_2 state of the oxygen-evolving complex of photosystem II. *Chem.—Eur. J. 16*, 10424−10438.

(121) Pantazis, D. A., Orio, M., Petrenko, T., Zein, S., Lubitz, W., Messinger, J., and Neese, F. (2009) Structure of the oxygen-evolving complex of photosystem II: Information on the S_2 state through quantum chemical calculation of its magnetic properties. *Phys. Chem. Chem. Phys. 11*, 6788−6798.

(122) Pantazis, D. A., Orio, M., Petrenko, T., Zein, S., Bill, E., Lubitz, W., Messinger, J., and Neese, F. (2009) A new quantum chemical approach to the magnetic properties of oligonuclear transition-metal complexes: Application to a model for the tetranuclear manganese cluster of photosystem II. *Chem.—Eur. J. 15*, 5108−5123.